PGE₂ attenuates liver fibrosis in mice by downregulating miR-23a-5p and inducing apoptosis of hepatic stellate cells.

[1]Brea R., [1]Motiño O., [2]Francés D., [3]García-Monzón C., [3]Vargas J., [4]Fernández-Velasco M., [1,5,6]Boscá L., [5,6,7]Casado M., *[1,5,6] Martín-Sanz P. & *[1]Agra N.

Affiliations

[1]Instituto de Investigaciones Biomédicas (IIB) "Alberto Sols", CSIC-UAM, Arturo Duperier 4, 28029 Madrid, Spain; [2]Instituto de Fisiología Experimental (IFISE-CONICET), Suipacha 570, 2000 Rosario, Argentina; [3]Liver Research Unit, Hospital Universitario Santa Cristina, Instituto de Investigación Sanitaria Princesa, Amadeo Vives 2, 28009 Madrid, Spain; [4]Instituto de Investigación Hospital Universitario La Paz, IDIPAZ, Pedro Rico 6, 28029 Madrid, Spain; [5]Centro de Investigación Biomédica en Red de Enfermedades Hepáticas y Digestivas (CIBERehd) y [6]Centro de Investigación Biomédica en Red de Enfermedades Cardiovasculares (CIBERcv), Monforte de Lemos 3-5, 28029 Madrid, Spain; [7]Instituto de Biomedicina de Valencia, IBV-CSIC, Jaume Roig 11, 46010 Valencia, Spain.

* Corresponding authors

These two authors share senior authorship (*)

Keywords: COX-2, Liver, HSC, miRNAs, Fibrosis

Contact Information:

Dr. Noelia Agra Instituto de Investigaciones Biomédicas (IIB) "Alberto Sols", CSIC-UAM. Madrid. Arturo Duperier, 4 28029 Madrid, Spain; Tel 34912071010 Ext 228 Fax: 34912071061 e-mail: noelia.agra@gmail.com or Dr. Paloma Martín-Sanz, Instituto de Investigaciones Biomédicas (IIB) "Alberto Sols", CSIC-UAM. Madrid. Arturo Duperier, 4 28029 Madrid, Spain; Tel 34914972746 Fax: 34915854401; e-mail: pmartins@iib.uam.es

List of Abbreviations:

COX-2, cyclooxygenase-2; PGE_2, prostaglandin E_2; ALT, alanine transaminase; TGF-β1, transforming growth factor β1; Bax, Bcl-2-associated X protein; Bcl-x_L, B-cell lymphoma-extra-large; α-SMA, alpha smooth muscle actin; COL1A1, collagen type I alpha 1; NAFLD, non-alcoholic fatty liver disease; NASH, non-alcoholic steatohepatitis; PCNA, proliferating cell nuclear antigen; ERK1, extracellular signal-regulated kinase 1; Bmp2, bone morphogenic protein 2; CDH1, E-Cadherin; Alf2, transcription factor 3; p38, mitogen-activated protein kinase 14; Fn1, fibronectin 1; Apaf1, apoptotic peptidase activating factor 1; Tradd, TNFRSF1A-associated via death domain, Cav1, caveolin 1.

ABSTRACT

MicroRNAs (miRNAs), small noncoding RNAs modulating messenger RNA (mRNA) and protein expression, have emerged as key regulatory molecules in chronic liver diseases, whose end stage is hepatic fibrosis, a major global health burden. Pharmacological strategies for prevention or treatment of hepatic fibrosis are still limited, what makes it necessary to establish a better understanding of the molecular mechanisms underlying its pathogenesis. In this context, we have recently shown that cyclooxygenase-2 (COX-2) expression in hepatocytes restricts activation of hepatic stellate cells (HSCs), a pivotal event in the initiation and progression of hepatic fibrosis. Here, we evaluated the role of COX-2 in the regulation of a specific set of miRNAs on a mouse model of CCl_4 and bile duct ligation (BDL)-induced liver fibrosis. Our results provide evidence that COX-2 represses miR-23a-5p and miR-28-5p expression in HSC. The decrease of miR-23a-5p and miR-28-5p expression promotes protection against fibrosis by decreasing the levels of pro-fibrogenic markers α-SMA and COL1A1 and increasing apoptosis of HSC. Moreover, we demonstrate that serum levels of miR-28-5p are decreased in patients with chronic liver disease. These results suggest a protective effect exerted by COX-2-derived prostanoids in the process of hepatofibrogenesis.

1. INTRODUCTION

Cyclooxygenase-1 (COX-1) and -2 catalyze the first step in prostanoid biosynthesis. COX-1 is constitutively expressed in many tissues, whereas COX-2 is induced by a variety of stimuli [1]. Adult hepatocytes fail to induce COX-2 expression regardless of the pro-inflammatory factors used [2]. However, our group and others demonstrated that partial hepatectomy (PH) induced COX-2 in hepatocytes and contributed to the progression of cell cycle during regeneration [3]. In addition, COX-2 is up-regulated in the livers of patients with chronic viral hepatitis, cirrhosis and hepatocellular carcinoma (HCC), and this upregulation leads to increased production of prostaglandins, mainly PGE_2 [4].

Liver fibrosis is characterized by an excessive accumulation of extracellular matrix (ECM) proteins in response to chronic hepatic injury [5]. Hepatic stellate cells (HSC) have been recognized as the principal cell type responsible for ECM formation during hepatic fibrogenesis and TGF-β represents one key factor stimulating collagen and ECM production in these cells [6]. Induction of α-smooth muscle actin (α–SMA) is the most reliable marker of HSC activation [7]. Moreover, hepatic TGF-β1 is increased in animal models of liver fibrosis and in patients with chronic liver diseases [8] and has been inversely correlated to PGE_2 action over HSCs activation [9].

miRNAs are small non-coding RNAs that negatively regulate their target genes primarily through RNA destabilization or translational repression. Aberrant miRNA expression is associated with pathologic conditions. In the context of liver diseases, previous studies revealed a role for miRNAs in acute liver injury, viral hepatitis, hepatocarcinogenesis, hepatic fibrosis and NAFLD [10–12]. Up to now, several miRNAs are known to affect different steps of fibrogenesis including HSC activation, proliferation, migration, and ECM

deposition. Members of the miR-29 family are downregulated in HSCs in response to TNF-α and TGF-β signaling and suppress the transcription of ECM genes like *Col1a1* [13]. miR-133a and miR-101 are other miRNAs regulated by TGF-β in HSCs, influencing ECM-related gene translation in liver fibrosis [14]. Next to these antifibrotic miRNAs, several pro-fibrotic miRNAs are up-regulated during fibrogenesis: elevated expression of miR-21 enhances HSC-activation and EMT by activating the PTEN/Akt pathway [15]. Moreover, TGF-β induced up-regulation of both miR-199s and miR-200 that indirectly promotes liver fibrosis by increasing the expression of pro-fibrotic genes (e.g. collagens, MMPs) [16].

Regarding COX-2 and the impact of PGE_2 on the development of fibrosis the data are controversial. Some studies indicate that PGs favor the development of hepatic steatosis, NASH and ultimately fibrosis [17–19], whilst others provide evidence that PGE_2 suppresses fibrogenesis and NASH progression since COX-2 inhibition potentiates inflammation and liver fibrosis [9,20,21]. Our results indicate that constitutive expression of COX-2 in hepatocytes protects against high fat diet-induced steatosis, inflammation, obesity and insulin resistance [22]. These findings prompted us to screen the role of hepatic-specific COX-2 expression in a murine model of fibrosis induced by CCl_4. In our previous work we have demonstrated that expression of COX-2 in hepatocytes was able to diminish the levels of pro-fibrogenic markers and to reduce the progression of the CCl_4-induced fibrotic process by restricting HSC activation and ECM deposition [23], but the involvement of miRNAs has not been analyzed previously. In this study, we examine a group of miRNAs that were modulated in HSC in response to COX-2 hepatocyte-specific expression. miR-23a and miR-28a were found to be downregulated by PGE_2 in a TGF-β-dependent manner, which could attenuates the activation of HSCs, with growth-suppressive and pro-apoptotic

5

activities. Moreover, we demonstrate that serum levels of miR-28 decreased in patients with chronic liver disease. Based on our findings, we propose that miR-23a and miR-28a are part of a novel signaling pathway that mediates a COX-2-dependent protective role by modulating the activation and apoptosis of HSC during hepatofibrogenesis.

2. EXPERIMENTAL PROCEDURES

2.1 Animal experimentation

hCOX-2-Tg mice and their corresponding wild type (Wt) litter-mates were generated by systematic mating of the heterozygous B6D2-Tg (APOE-PTGS2/4)Upme expressing 55 copies of transgene with B6D2F1/OlaHsd Wt mice in our animal house for more than seven generations. The hCOX-2-Tg animals were phenotypically similar to their normal litter-mates and did not exhibit a detectable histological change in the liver at 12-weeks of age. Integration of transgene was systematically checked by PCR analysis of genomic tail DNA. Transgenic mice (hCOX-2-Tg) constitutively express human COX-2 in hepatocytes under the control of the human ApoE promoter and its specific hepatic control region (HCR), a unique regulatory domain that directs ApoE expression in liver [24], lacking macrophage-specific regulatory regions (ME.2 and ME.1) [25]. The animals were maintained in light/dark (12 h light/12 h dark), temperature (22 °C) and humidity-controlled rooms with free access to drinking water. Mice were fed with regular chow diet (RCD; SAFE A04-10 Panlab, Barcelona). To induce fibrosis, CCl_4 (1:4 in olive oil) was intraperitoneally (i.p.) administered to hCOX-2-Tg and Wt mice at a dose of 1.6 ml/kg body weight twice-weekly. Control animals were i.p. injected with olive oil. In another approach to induce fibrosis, some animals were subjected to bile duct ligation (BDL) for 21 days. 9 weeks after CCl_4 treatment or 21 days after BDL, the animals were sacrificed and liver was snap-frozen in liquid nitrogen and stored at -80°C for further mRNA analysis, or fixed in 4% buffered formalin to later make paraffin blocks. Plasma was obtained from retro-orbital sinus.

All animal experimentation was controlled following the recommendations of the Federation of European Laboratory Animal Science Associations (FELASA) on health

monitoring, the European Community Law (86/609/EEC) and the Spanish Law (R.D.1201/2005), and the use of animals in experimental procedures was approved by the Ethics Committee of the Bioethical Commission from CSIC, Spain.

Histochemistry analysis, immunoblot assays, RNA isolation and real-time RT-PCR; hepatic cell isolation and other *in vivo* and *in vitro* experimental procedures are detailed in the Supplementary data section.

2.2 Isolation and culture of hepatic stellate cells (HSC)

The isolation of HSCs from mice livers was performed as described [26] and can be divided into: *In situ* perfusion with pronase (0.4 mg/ml)/collagenase (0.56 mg/ml, increasing 1.5-fold after CCl_4 treatment) solution in William's E medium of mouse liver; subsequent *in vitro* digestion; and density gradient–based separation of HSCs from other hepatic cell populations. Briefly, after the *in situ* digestion, the liver was carefully removed and minced under sterile conditions. The minced liver was further digested *in vitro* with pre-warmed pronase (0.5 mg/ml)/collagenase (0.4 mg/ml)/DNase I (0.1 mg/ml)/HEPES (10 mM) in 1X HBSS pH 7.4 solution. Then, the liver cell suspension was filtered through a 100 μm cell strainer to eliminate undigested tissue remnants and centrifuged at 1900 rpm for 10 min at 4°C. The pellet of non-parenchymal cells was resuspended in GBSS (Sigma) and purified by density gradient centrifugation using 14% Nycodenz (Sigma). HSC cells were collected from the diffuse white interphase layer and centrifuged twice in 1X PBS/0.3% BSA at 1900 rpm for 5 min at 4ºC. Cells were resuspended directly in 700 μl QIAzol Lysis Reagent (Qiagen) for further mRNA analysis or were plated in 6 or 12 multiwell dishes (Corning, New York, USA) with DMEM, 20% FBS and 100 U/ml penicillin, 100 µg/ml streptomycin and 50 µg/ml gentamicin. Cells were cultured to further

mRNA and protein analysis. A primary HSC cell line from Wt mice was established by spontaneous immortalization.

2.3 miRNA microarray analysis

miRNAs from 26 Wt and 21 COX-2-Tg isolated HSC samples were extracted using QIAzol Lysis Reagent (Qiagen, Valencia, CA) and purified with a miRNeasy Mini Kit (Qiagen) after oil or CCl_4 treatment. The quality and integrity of the microRNAs were assessed in an Agilent Bioanalyzer. For miRNA array analysis, we used a miRCURY LNA™ Universal RT microRNA PCR, 4x Mouse & Rat panel I+II (Exiqon). It contains pre-aliquoted PCR primer sets in 384-well PCR plates, allowing the study of 748 mouse and rat microRNAs and 6 reference genes.

For cDNA synthesis, RNA (5 ng/µl) was polyadenylated and reverse transcribed to cDNA using a Universal cDNA Synthesis Kit II (Part from miRCURY LNA^{TM} Universal RT microRNA PCR, Exiqon), according to the manufacturer´s instructions. cDNAs were diluted 80x and were used as the template for quantitative real-time PCR (RT-PCR). ExiLENT SYBR$^{®}$ Green master mix (Exiqon), loaded into pre-aliquoted PCR primer sets in 384-well PCR plates. RT-PCR was performed with a 7900HT Fast-Real Time PCR System (Life Technologies), and the thermocycling parameters were 95°C for 10 min and 40 cycles of 95°C for 10 s and 60°C for 1 min; followed by a dissociation curve consisting of 95ºC for 15 s; 60ºC for 15 s; 95ºC for 15 s. The mean of triplicate probes was used for each array, and expressed data were normalized using the mean normalization method. The fold change in expression level of each miRNA was determined by comparing the expression levels of miRNAs in COX-2-Tg cells to those in Wt cells. Data analysis was

performed using GenEx2.0 Software. The Heatmaps and clustering of differentially expressed genes were constructed in Excel using conditional formatting.

Microarray data were validated by RT-PCR analysis of individual miRNAs. Analysis of pathways, networks and target genes was performed using miRWalk and "Database for Annotation, Visualization and Integrated Discovery" (DAVID: Functional Annotation Tools) platforms, allowing the identification of several candidate pathways for the miRNA target genes. Cytoskape software was used to illustrate the overlap of the putative miRNAs targets.

2.4 Data analysis

Data are expressed as means $\pm$ S.E of at least three independent experiments. Statistical significance was estimated using Student 2-tailed t-test to evaluate the differences between treated and untreated mice or cells within a single genotype and between genotypes. Analysis was performed by using the statistical software GraphPad Prism 5. A $P < 0.05$ was considered statistically significant.

3. RESULTS

3.1 miR-23a and miR-28a are specifically repressed by COX-2-derived prostanoids in hepatic stellate cells upon induction of liver fibrosis.

To investigate the role of COX-2 activity on fibrosis, we injected CCl_4 in Wt and hCOX-2-Tg mice twice a week for 9 weeks. Liver sections were stained with hematoxylin and eosin (H&E), Masson's trichrome (MTC) and Picro Sirius Red to evaluate the fibrosis stage and to quantify the fibrotic area. We found a delayed progression in fibrosis in hCOX-2-Tg mice (Supplementary Fig.1A-C) as well as in isolated HSC cells from hCOX-2-Tg *vs.* Wt mice treated with CCl_4 (Supplementary Fig. 1D-E) in agreement with our previous results [23]. Since we have demonstrated that COX-2 regulates miRNA processing [27], here we sought to analyze whether miRNAs might be implicated in the COX-2-dependent attenuation of fibrosis.

As CCl_4 is the condition leading to fibrosis, we will compare the hCOX-2-Tg *vs.* Wt under CCl_4 condition. Microarray analysis in HSC (the most important source of ECM) revealed that in CCl_4 mice, the expression level of 11 miRNAs was downregulated in hCOX-2-Tg mice *vs.* Wt mice, while the expression of miR-29a was higher (P ≤0.05; fold change cutoff ≥1.5) (Fig. 1A). According to previous results, it is well established the powerful anti-fibrotic role of miR-29 in different mouse models of liver fibrosis and in different species including human. Besides, members of the miR-199-family have a pro-fibrotic effect since they are increased in fibrotic liver diseases in both mouse and human [12]. These two miRNAs, along with the two most statistically significant (miR-23a and miR-28a), were chosen to validate the microarray results using real-time qPCR and these data supported the result of the microarray analysis (data not shown).

To determine an HSC-specific role for miR-23a and miR-28 in liver fibrosis, the expression levels of these two miRNAs were examined in primary HSCs isolated from the livers of hCOX-2-Tg mice after 9 weeks of CCl_4 treatment, as well as from Wt mice. The expression of miR-29a and miR-199a was also analyzed. In HSCs from hCOX-2-Tg mice with liver fibrosis, we found a substantial downregulation of miR-23a, miR-28a and miR-199a *vs*. Wt (Fig. 1B), contrary to what happens in hepatocytes (Fig. 1C). We failed to detect significant differences of miR-23 and miR-28 in total liver and Kupffer cells isolated from fibrotic liver of Wt and Tg mice (Fig. 1D, E).

3.2 PGE₂ attenuates TGF-β-dependent increase of miRNA expression in HSC cells.

As miR-23a and miR-28a exhibited a consistent downregulation in HSCs from fibrotic hCOX-2-Tg mice and they were not examined in this context in previous analyses, these miRNAs were selected for further evaluation.

First we investigated whether PGE_2 affects TGF-β-induced HSC activation by regulating miR-23a and miR-28a expression. RT-PCR results demonstrated that PGE_2 significantly decreased the TGF-β1-dependent rise of miR-23a and miR-28a in isolated HSC cells from Wt mice, as well as in human and murine HSC cell lines, LX2 and GRX, respectively, treated with PGE_2 after TGF-β1 in comparison with cells activated with TGF-β1. (Fig.2A-C). Our results validate the upregulation of pro-fibrogenic genes upon TGF-β1 treatment and revealed that PGE_2 counteracted TGF-β1-induction of α-SMA and COL1A1 (Fig. 2D). To determine whether PGE_2 exerts its effects via the TGF-β1 classical signaling pathway, we treated HSC with LY364947, an inhibitor of TRβ-I. Interestingly, LY364947 significantly prevented the PGE_2 dependent downregulation of miR-23a and miR-28a (Fig.

2E). These data highlight a potential role for TGF-β1 in the HSC specific regulation of miR-23a and miR-28a by PGE_2 in the process of fibrosis.

3.3 COX-2-Tg mice subjected to bile duct ligation are protected against fibrosis.

To confirm our results, we next used a second model of experimental liver fibrosis and analyzed the expression of miR-23a and miR-28a, 21 days after bile duct ligation (BDL) in Wt and hCOX-2-Tg mice. The degree of liver fibrosis was determined by H&E, Picrosirius red and Masson's staining. Histopathological analysis revealed that BDL caused significant bridging fibrosis, but PGE_2 synthesis caused marked reduction in the distribution of collagen fibers in the fibrotic liver of hCOX-2-Tg mice. (Fig. 3A). These results, together with the ALT values, confirm the hepatoprotective role of COX-2 on the BDL-induced liver fibrosis in mice (Fig. 3B). As shown in figure 3C, miR-23a and miR-28a were downregulated in Tg *vs.* Wt animals, further supporting the hypothesis that downregulation of miR-23a and miR-28a by PGE_2 constitutes an important feature in murine fibrosis. Immunohistochemical results demonstrated that the levels of α-SMA in BDL mice were higher compared with the sham-operated mice, and attenuated in the presence of COX-2 (Fig. 3D).

3.4 Relationship between COX-2-regulated miRNAs, TGF-β1 and apoptosis pathways.

To further characterize the functional significance of the differentially miRNAs regulated by COX-2, we performed a systematic analysis of their putative gene targets and searched for pathways which were enriched. Putative target genes were identified by using www.microrna.org, a well-established target prediction algorithm for miRNAs. To interpret the biological effect of miR-23a and miR-28a, genes obtained in this analysis were further processed by DAVID 6.7 software for functional pathway enrichment. Various targets of

these miRNAs were significantly enriched in different Kyoto Encyclopedia of Genes and Genomes (KEGG) pathways using corrected P value ≤ 0.05 as a threshold, including the top hit ´pathways in cancer´, but also ´focal adhesion´, ´apoptosis´, ´TGF-β signaling pathway´ and other potentially involved in liver fibrosis (Fig. 4A), suggesting that fibrosis-relevant target genes might be regulated by the putative network of PGE_2/TGF-β1-dependent miRNAs in HSCs. A total of 10 genes were selected to illustrate the overlap of the COX-2-regulated miRNA target genes. These 10 genes belonged to the affected pathways including apoptosis and TGF-β signaling pathway (Fig. 4B).

The deregulation of these putative target genes was finally confirmed by RT-PCR in different HSC cell models: HSC isolated from Wt and hCOX-2-Tg livers treated with CCl_4 and Wt HSC treated with PGE_2 and TGF-β1. The results confirmed the upregulation of these potential target genes in HSCs in the presence of PGE_2, upon CCl_4 or TGF-β1 treatment (Fig. 4C). Furthermore, the expression of target genes was downregulated when HSC cells were transfected with miR-23a and miR-28a (Fig. 4D).

3.5 PGE_2 reduced the activation of hepatic stellate cells in vitro.

Given the crucial role of COX-2 in suppressing liver fibrosis *in vivo*, we examined whether PGE_2 contributes to modulation of the activation of HSC *in vitro*. HSC were treated with conditioned medium of hepatocytes isolated from Wt and hCOX-2-Tg mice after Oil or CCl_4 treatment. As shown in Fig. 5B, PGE_2 levels were higher in the culture media from Tg hepatocytes. This approach resembles what occurs physiologically in Tg mice. Pro-fibrogenic markers such as α-SMA and COL1A1, were measured by immunofluorescence and as shown in Fig. 5A, HSC-Tg and HSC-Tg-CCl_4 cells showed lesser levels of both

markers confirming our previous results [23]. Moreover, pSmad2/3 was decreased in HSC-Tg-CCl_4 cells in comparison with Wt- CCl_4 (Fig. 5C).

3.6 PGE$_2$ has a growth-suppressive and pro-apoptotic role in HSC cells.

We then investigated the effects of PGE$_2$ on HSC proliferation and apoptosis. We found that PGE$_2$ decreases the CCl_4-induced Ki-67 and PCNA expression, markers of cell proliferation (Fig. 6A). Moreover, as determined by the MTT cell viability assay, incubation with conditioned media from Tg mice hepatocytes caused a significant inhibition of HSC cell proliferation (Fig. 6B).

To determine whether the observed suppressive effect of cell growth by PGE$_2$ was due to an induction of apoptosis, cell death was evaluated by immunostaining of the pro-apoptotic proteins Bax and cleaved caspase-3, showing that expression of COX-2 in hepatocytes led to an increase expression of these pro-apoptotic markers in HSC (Fig. 6C, D and Supplementary Fig.2). These findings indicate that PGE$_2$ induces cell death and reduces subsequent proliferative activity specifically in HSCs.

3.7 Ectopic expression of miR-23a and miR-28a induced HSC cell activation

Next, we transiently transfected HSC with a vector expressing miR-23a and miR-28 separately or in combination (Supplementary Fig.3A-B). As shown in Fig. 7A, the transfection with miR-23a significantly increased α-SMA and COL1A1 protein levels in HSCs, reflecting their pro-fibrotic function. We analyzed a potential additive effect of miR-23a and miR-28a on the expression of fibrotic markers. Co-transfection of miR-23a and miR-28a into HSC did not show a synergistic effect. Furthermore, overexpression of miR-23a and miR-28a counteracted the effect of PGE$_2$ on the expression of α-SMA and COL1A1 after TGF-β1 treatment of HSCs, further highlighting the role of these miRNAs

15

in the regulation of collagen during hepatofibrogenesis (Fig. 7B). Next, we measured ERK1, BMP2 and CDH1 protein levels, target genes implicated in apoptosis, TGF-β signaling and focal adhesion pathways identified in Fig.4, and as expected these proteins were increased in HSC cells stimulated with PGE$_2$ after TGF-β1 compared with TGF-β1. Transfection with miR-23a and miR-28a reversed this effect (Fig. 7B). In cells transfected with miR-23a and/or miR-28a, we observed a significant increase in cell viability compared with cells transfected with control miRNA and treated with PGE$_2$ and TGF-β1, as assessed by MTT cell viability assays (Fig. 7C). Moreover, the overexpression of these miRNAs reduced the apoptosis, as measured by cleaved caspase-3 and Bcl-xL protein levels, opposite to the effect of PGE$_2$ (Fig. 7D).

3.8 Serum levels of miR-23a and miR-28a are differentially regulated in patients with liver fibrosis.

We analyze miRNAs expression in serum of 25 non-diabetic patients with a clinical diagnosis of fibrosis (grade I-III), who underwent a liver biopsy for diagnostic purposes, and compared them to the sera of 13 healthy controls (normal liver, NL) (Supplementary Fig. 4A). There was a reduction in the expression of miR-28a with the progression of hepatic fibrosis in relation to the increase levels of PGE$_2$ (Supplementary Fig. 4A-C), suggesting there might be a similar regulation and function of miR-28a in human fibrogenesis and in murine experimental fibrotic process.

4. DISCUSSION

The current report proposes a novel miRNA-dependent mechanism by which COX-2 modulates liver fibrosis. Hepatocyte COX-2 expression represses miR-23a-5p and miR-28a-5p expression in HSC and exerts a protective effect in the process of liver fibrosis through the activation of apoptosis and the decrease in pro-fibrogenic markers.

Liver injury leading to fibrosis occurs in response to a variety of insults including alcohol, viral hepatitis, steatosis and insulin resistance. Fibrosis is the consequence of an overactive wound healing process in response to the injury. Initially, this process is driven by an inflammatory response and results in a controlled deposition of extracellular matrix; however, if the underlying insult persists, there is an excessive deposition of extracellular matrix including cross-linking of collagen. The critical step in the development of scar is activation of hepatic stellate cells (HSCs), which become the primary source of extracellular matrix [28].

miRNAs play essential roles in virtually all cellular and biological processes including liver development, differentiation and homeostasis. Altered expression levels of miRNAs were observed in patients with liver diseases e.g. liver steatosis, cirrhosis and hepatocellular carcinoma [10–12,29]. Expression pattern of miRNAs are organ- and cell-specific. In the liver, miRNAs are not homogeneously distributed but are selectively expressed and regulated in distinct hepatic cell types. For certain miRNAs, opposite regulation were described between the different liver cell compartments. As an example, expression of miR-29, one of the best studied miRNAs in liver diseases, was found to be down-regulated in HSCs during hepatofibrogenesis, while its expression was up-regulated in hepatocytes and cholangiocytes during experimental biliary atresia, supporting the concept of cell-

specific functions of miRNAs in liver pathophysiology. This is in agreement with our results showing opposite regulation of miR-23a and miR-28a in HSCs compared to hepatocytes [30]. In addition, our results showing an antifibrotic role of miR-29a are widely supported by the literature. Wang. *et al.,* demonstrated that miR-29 attenuated HSC activation and induced their apoptosis *via* inhibition of PI3K/AKT pathway in CCl_4-induced fibrosis mouse [31]. Moreover, systemic injection of miR-29a expressing adeno-associated virus in mice demonstrated reversal of histologic and biochemical evidence of hepatic fibrosis despite continued exposure to CCl_4 [32].

The role of COX-2 dependent PGs in liver fibrosis is controversial. Some studies indicate that PGs favor the development of hepatic steatosis, NASH and ultimately fibrosis [17–19], whilst others provide evidence that PGE_2 suppresses fibrogenesis [9,20,21]. The discrepancy on the effect of COX-2 function can partly be attributed to the application of different experimental models. COX-2 inhibitors could also influence gene expression via COX-2-independent pathways. To overcome the limitations of pharmacological inhibition of COX-2, we used a Tg mice model with enhanced hepatocyte-specific hCOX-2 expression. We found that in Tg mice, the severity of hepatic fibrosis developed after CCl_4 was lesser than in Wt mice, as demonstrated by reduced degree of fibrosis, HSC activation and proliferation as well as increased HSC apoptosis. Also our results show that miR-23a and miR-28a are downstream effectors participating in COX-2 function during fibrogenesis.

We analyzed the enriched signaling pathways among the predicted targets of the miRNAs regulated by COX-2 in HSC cells and focused in apoptosis and TGF-β signaling, based on our previous results indicating that hepatocyte COX-2 expression ameliorates NASH and

liver fibrosis development in mice by reducing inflammation, oxidative stress and apoptosis and by modulating activation of HSC [23]. Some of these miRNA target genes were validated by RT-PCR and *Erk1, Bmp2, Cav-1* and *Cdh1* exhibited increased expression in isolated HSC from COX-2-Tg liver treated with CCl_4 as well as in HSC incubated with TGF-β and PGE_2. All these genes have antifibrotic and pro-apoptotic functions [33].

It has been described that COL1A2 is downregulated in fibroblast-derived extracellular matrix via Ras-dependent activation of the MEK/ERK signaling pathway and that Sp1 is an important mediator of this feedback inhibition [34]. Moreover, in a different context of cartilage degradation, sphingomyelinase treatment of chondrocytes decreases type II collagen via activation of the ERK signaling cascade, redistribution of SOX9 and recruitment of c-Fos [35]. Bone morphogenetic proteins (BMPs), members of the TGF-β superfamily, have anti-fibrotic functions in multiple organs. BMP2 opposes the fibrogenic function of TGF-β in pancreatic stellate cells through the Smad1 signaling pathway, inhibiting TGF-β-induced α-SMA and COL1A1 [36] and inducing apoptosis in mouse hybridoma MH60 cells through the activation of TGFβ-activated kinase (TAK1) and subsequent phosphorylation of p38 stress-activated protein kinase [37]. Regarding caveolin-1 (CAV-1), our results agree with *in vitro* data for the fibromir miR-199a-5p, which is regulated by TGF-β signaling in response to lung injury. Specifically, miR-199a targets CAV-1, a potent negative regulator of TGF-β signaling cascade [38]. By other hand, CAV-1 overexpression resulted in inhibition of α-SMA expression and cell proliferation by blocking the progression through the G1 phase in murine fibroblast [39] and prevented the protease-activated receptor-2 (PAR2)-induced release of collagen as

well restored the apoptosis in human HSC line, HHStec cells [40]. Finally, it has been shown that an increase of E-cadherin expression promotes HSC apoptosis [41] and correlates with the inhibition of LX2 and HSC-T6 cell proliferation after icaritin treatment, a known apoptosis inducer of HSC [42].

Aberrant apoptosis is a feature of chronic liver diseases and is associated with worsening stages of fibrosis. After toxic exposure, hepatocytes undergo apoptosis and hepatic stellate cells migrate to the site of injury to engulf the apoptotic bodies. This engulfment promotes activation of the hepatic stellate cells to hepatic myofibroblasts, and in their activated state these cells promote deposition of extracellular matrix and scar formation in the liver. However, apoptosis is also the main mechanism promoting the resolution of fibrosis. When liver fibrosis resolves, the activated HSCs are either returning to a quiescent state or undergoing apoptosis, which causes a decrease in the number of activated HSCs [28].

4.1 Conclusions

Based on our results, we propose that hepatocyte COX-2 expression attenuates liver fibrosis in part through the production of PGE_2 which exerts its hepatoprotective role in at least two different ways: by decreasing hepatocyte apoptosis [23], thus reducing HSC activation; and by downregulation of miR-23a and miR-28a in HSC, decreasing proliferation and increasing its apoptosis, leading to fibrosis resolution (Fig. 8).

Moreover, in this study we detected significantly reduced serum levels of miR-28a in patients with liver fibrosis, and high serum PGE_2 levels were associated with the progression to more advanced fibrosis stages. We hypothesize this fact as a response in order to exert a protective role against liver fibrosis and contribute to its resolution.

Pharmacological strategies to prevent or treat liver fibrosis are still limited. The prospect of treating patients with liver disease with a pharmacological agent to cause the regression of fibrosis is exciting, but further investigation is required into the long-term-efficacy. The link between HSC specific downregulation of miR-23a and miR-28a by PGE_2 and their relation to ECM and apoptotic genes, as well as the prevention of HSCs activation exerted by PGE_2 highlight a potential role for these miRNAs in HSC and may provide further pharmacological targets.

Funding:

5. REFERENCES

[1]   E. Ricciotti, G.A. FitzGerald, Prostaglandins and inflammation, Arter. Thromb Vasc Biol. 31 (2011) 986–1000. doi:10.1161/ATVBAHA.110.207449.

[2]   P. Martin-Sanz, N.A. Callejas, M. Casado, M.J. Diaz-Guerra, L. Bosca, Expression of cyclooxygenase-2 in foetal rat hepatocytes stimulated with lipopolysaccharide and pro-inflammatory cytokines, Br J Pharmacol. 125 (1998) 1313–1319. doi:10.1038/sj.bjp.0702196.

[3]   M. Casado, N.A. Callejas, J. Rodrigo, X. Zhao, S.K. Dey, L. Boscá, P. Martín-Sanz, Contribution of cyclooxygenase 2 to liver regeneration after partial hepatectomy., FASEB J. 15 (2001) 2016–8. doi:10.1096/fj.01-0158fje.

[4]   A. Fernandez-Alvarez, C. Llorente-Izquierdo, R. Mayoral, N. Agra, L. Bosca, M. Casado, P. Martin-Sanz, Evaluation of epigenetic modulation of cyclooxygenase-2 as a prognostic marker for hepatocellular carcinoma, Oncogenesis. 1 (2012) e23. doi:10.1038/oncsis.2012.23.

[5]   R. Bataller, D.A. Brenner, Liver fibrosis, J Clin Invest. 115 (2005) 209–218. doi:10.1172/JCI24282.

[6]   F. Tacke, R. Weiskirchen, Update on hepatic stellate cells: pathogenic role in liver fibrosis and novel isolation techniques, Expert Rev Gastroenterol Hepatol. 6 (2012) 67–80. doi:10.1586/egh.11.92.

[7]   S.L. Friedman, Hepatic stellate cells: protean, multifunctional, and enigmatic cells of the liver, Physiol Rev. 88 (2008) 125–172. doi:10.1152/physrev.00013.2007.

[8]   A. Castilla, J. Prieto, N. Fausto, Transforming growth factors beta 1 and alpha in chronic liver disease. Effects of interferon alfa therapy, N Engl J Med. 324 (1991)

933–940. doi:10.1056/NEJM199104043241401.

[9]   A.Y. Hui, A.J. Dannenberg, J.J.Y. Sung, K. Subbaramaiah, B. Du, P. Olinga, S.L. Friedman, Prostaglandin E2 inhibits transforming growth factor beta 1-mediated induction of collagen alpha 1(I) in hepatic stellate cells., J. Hepatol. 41 (2004) 251–8. doi:10.1016/j.jhep.2004.04.033.

[10]   D.M.S. Ferreira, A.L. Simão, C.M.P. Rodrigues, R.E. Castro, Revisiting the metabolic syndrome and paving the way for microRNAs in non-alcoholic fatty liver disease., FEBS J. 281 (2014) 2503–24. doi:10.1111/febs.12806.

[11]   C. Roderburg, G.W. Urban, K. Bettermann, M. Vucur, H. Zimmermann, S. Schmidt, J. Janssen, C. Koppe, P. Knolle, M. Castoldi, F. Tacke, C. Trautwein, T. Luedde, Micro-RNA profiling reveals a role for miR-29 in human and murine liver fibrosis, Hepatology. 53 (2011) 209–218. doi:10.1002/hep.23922.

[12]   S. Roy, F. Benz, T. Luedde, C. Roderburg, The role of miRNAs in the regulation of inflammatory processes during hepatofibrogenesis, Hepatobiliary Surg Nutr. 4 (2015) 24–33. doi:10.3978/j.issn.2304-3881.2015.01.05.

[13]   S. Bandyopadhyay, R.C. Friedman, R.T. Marquez, K. Keck, B. Kong, M.S. Icardi, K.E. Brown, C.B. Burge, W.N. Schmidt, Y. Wang, A.P. McCaffrey, Hepatitis C virus infection and hepatic stellate cell activation downregulate miR-29: miR-29 overexpression reduces hepatitis C viral abundance in culture, J Infect Dis. 203 (2011) 1753–1762. doi:10.1093/infdis/jir186.

[14]   C. Roderburg, M. Luedde, D. Vargas Cardenas, M. Vucur, T. Mollnow, H.W. Zimmermann, A. Koch, C. Hellerbrand, R. Weiskirchen, N. Frey, F. Tacke, C. Trautwein, T. Luedde, miR-133a mediates TGF-beta-dependent derepression of

collagen synthesis in hepatic stellate cells during liver fibrosis, J Hepatol. 58 (2013) 736–742. doi:10.1016/j.jhep.2012.11.022.

[15]   J. Wei, L. Feng, Z. Li, G. Xu, X. Fan, MicroRNA-21 activates hepatic stellate cells via PTEN/Akt signaling, Biomed Pharmacother. 67 (2013) 387–392. doi:10.1016/j.biopha.2013.03.014.

[16]   M. Kitano, P.M. Bloomston, Hepatic Stellate Cells and microRNAs in Pathogenesis of Liver Fibrosis, J Clin Med. 5 (2016). doi:10.3390/jcm5030038.

[17]   S.M. Kim, K.C. Park, H.G. Kim, S.J. Han, Effect of selective cyclooxygenase-2 inhibitor meloxicam on liver fibrosis in rats with ligated common bile ducts, Hepatol Res. 38 (2008) 800–809. doi:10.1111/j.1872-034X.2008.00339.x.

[18]   Y.-H. Paik, J.K. Kim, J.I. Lee, S.H. Kang, D.Y. Kim, S.H. An, S.J. Lee, D.K. Lee, K.-H. Han, C.Y. Chon, S.I. Lee, K.S. Lee, D.A. Brenner, Celecoxib induces hepatic stellate cell apoptosis through inhibition of Akt activation and suppresses hepatic fibrosis in rats, Gut. 58 (2009) 1517–1527. doi:10.1136/gut.2008.157420.

[19]   J. Yu, E. Ip, A. Dela Pena, J.Y. Hou, J. Sesha, N. Pera, P. Hall, R. Kirsch, I. Leclercq, G.C. Farrell, COX-2 induction in mice with experimental nutritional steatohepatitis: Role as pro-inflammatory mediator, Hepatology. 43 (2006) 826–836. doi:10.1002/hep.21108.

[20]   A.Y. Hui, W.K. Leung, H.L. Chan, F.K. Chan, M.Y. Go, K.K. Chan, B.D. Tang, E.S. Chu, J.J. Sung, Effect of celecoxib on experimental liver fibrosis in rat, Liver Int. 26 (2006) 125–136. doi:10.1111/j.1478-3231.2005.01202.x.

[21]   Y. Kamada, K. Mori, H. Matsumoto, S. Kiso, Y. Yoshida, S. Shinzaki, N. Hiramatsu, M. Ishii, K. Moriwaki, N. Kawada, T. Takehara, E. Miyoshi, N-

Acetylglucosaminyltransferase V regulates TGF-beta response in hepatic stellate cells and the progression of steatohepatitis, Glycobiology. 22 (2012) 778–787. doi:10.1093/glycob/cws012.

[22] D.E. Frances, O. Motino, N. Agra, A. Gonzalez-Rodriguez, A. Fernandez-Alvarez, C. Cucarella, R. Mayoral, L. Castro-Sanchez, E. Garcia-Casarrubios, L. Bosca, C.E. Carnovale, M. Casado, A.M. Valverde, P. Martin-Sanz, Hepatic cyclooxygenase-2 expression protects against diet-induced steatosis, obesity, and insulin resistance, Diabetes. 64 (2015) 1522–1531. doi:10.2337/db14-0979.

[23] O. Motino, N. Agra, R. Brea Contreras, M. Dominguez-Moreno, C. Garcia-Monzon, J. Vargas-Castrillon, C.E. Carnovale, L. Bosca, M. Casado, R. Mayoral, M.P. Valdecantos, A.M. Valverde, D.E. Frances, P. Martin-Sanz, Cyclooxygenase-2 expression in hepatocytes attenuates non-alcoholic steatohepatitis and liver fibrosis in mice, Biochim Biophys Acta. 1862 (2016) 1710–1723. doi:10.1016/j.bbadis.2016.06.009.

[24] M. Casado, B. Mollá, R. Roy, A. Fernández-Martínez, C. Cucarella, R. Mayoral, L. Boscá, P. Martín-Sanz, Protection against Fas-induced liver apoptosis in transgenic mice expressing cyclooxygenase 2 in hepatocytes., Hepatology. 45 (2007) 631–8. doi:10.1002/hep.21556.

[25] V.G. Trusca, E.V. Fuior, I.C. Florea, D. Kardassis, M. Simionescu, A.V. Gafencu, Macrophage-specific up-regulation of apolipoprotein E gene expression by STAT1 is achieved via long range genomic interactions., J. Biol. Chem. 286 (2011) 13891–904. doi:10.1074/jbc.M110.179572.

[26] I. Mederacke, D.H. Dapito, S. Affo, H. Uchinami, R.F. Schwabe, High-yield and

high-purity isolation of hepatic stellate cells from normal and fibrotic mouse livers, Nat Protoc. 10 (2015) 305–315. doi:10.1038/nprot.2015.017.

[27]   O. Motino, D.E. Frances, R. Mayoral, L. Castro-Sanchez, M. Fernandez-Velasco, L. Bosca, C. Garcia-Monzon, R. Brea, M. Casado, N. Agra, P. Martin-Sanz, Regulation of MicroRNA 183 by Cyclooxygenase 2 in Liver Is DEAD-Box Helicase p68 (DDX5) Dependent: Role in Insulin Signaling, Mol Cell Biol. 35 (2015) 2554–2567. doi:10.1128/MCB.00198-15.

[28]   J.B. Chakraborty, F. Oakley, M.J. Walsh, Mechanisms and biomarkers of apoptosis in liver disease and fibrosis, Int J Hepatol. 2012 (2012) 648915. doi:10.1155/2012/648915.

[29]   X. Chen, Y. Zhao, F. Wang, Y. Bei, J. Xiao, C. Yang, MicroRNAs in Liver Regeneration., Cell. Physiol. Biochem. 37 (2015) 615–28. doi:10.1159/000430381.

[30]   C. Roderburg, C. Trautwein, Cell-specific functions of miRNA in the liver, J Hepatol. 66 (2017) 655–656. doi:10.1016/j.jhep.2016.09.015.

[31]   J. Wang, E.S. Chu, H.Y. Chen, K. Man, M.Y. Go, X.R. Huang, H.Y. Lan, J.J. Sung, J. Yu, microRNA-29b prevents liver fibrosis by attenuating hepatic stellate cell activation and inducing apoptosis through targeting PI3K/AKT pathway, Oncotarget. 6 (2015) 7325–7338. doi:10.18632/oncotarget.2621.

[32]   M.K. Knabel, K. Ramachandran, S. Karhadkar, H.W. Hwang, T.J. Creamer, R.R. Chivukula, F. Sheikh, K.R. Clark, M. Torbenson, R.A. Montgomery, A.M. Cameron, J.T. Mendell, D.S. Warren, Systemic Delivery of scAAV8-Encoded MiR-29a Ameliorates Hepatic Fibrosis in Carbon Tetrachloride-Treated Mice, PLoS One. 10 (2015) e0124411. doi:10.1371/journal.pone.0124411.

[33] S. Cagnol, J.C. Chambard, ERK and cell death: mechanisms of ERK-induced cell death--apoptosis, autophagy and senescence, FEBS J. 277 (2010) 2–21. doi:10.1111/j.1742-4658.2009.07366.x.

[34] K. Dzobo, V.D. Leaner, M.I. Parker, Feedback regulation of the α2(1) collagen gene via the Mek-Erk signaling pathway., IUBMB Life. 64 (2012) 87–98. doi:10.1002/iub.568.

[35] S.J. Gilbert, E.J. Blain, V.C. Duance, D.J. Mason, Sphingomyelinase decreases type II collagen expression in bovine articular cartilage chondrocytes via the ERK signaling pathway., Arthritis Rheum. 58 (2008) 209–20. doi:10.1002/art.23172.

[36] X. Gao, Y. Cao, W. Yang, C. Duan, J.F. Aronson, C. Rastellini, C. Chao, M.R. Hellmich, T.C. Ko, BMP2 inhibits TGF-beta-induced pancreatic stellate cell activation and extracellular matrix formation, Am J Physiol Gastrointest Liver Physiol. 304 (2013) G804-13. doi:10.1152/ajpgi.00306.2012.

[37] N. Kimura, R. Matsuo, H. Shibuya, K. Nakashima, T. Taga, BMP2-induced apoptosis is mediated by activation of the TAK1-p38 kinase pathway that is negatively regulated by Smad6, J Biol Chem. 275 (2000) 17647–17652. doi:10.1074/jbc.M908622199.

[38] C.L. Lino Cardenas, I.S. Henaoui, E. Courcot, C. Roderburg, C. Cauffiez, S. Aubert, M.C. Copin, B. Wallaert, F. Glowacki, E. Dewaeles, J. Milosevic, J. Maurizio, J. Tedrow, B. Marcet, J.M. Lo-Guidice, N. Kaminski, P. Barbry, T. Luedde, M. Perrais, B. Mari, N. Pottier, miR-199a-5p Is upregulated during fibrogenic response to tissue injury and mediates TGFbeta-induced lung fibroblast activation by targeting caveolin-1, PLoS Genet. 9 (2013) e1003291. doi:10.1371/journal.pgen.1003291.

[39]   D. Gvaramia, M.E. Blaauboer, R. Hanemaaijer, V. Everts, Role of caveolin-1 in fibrotic diseases, Matrix Biol. 32 (2013) 307–315. doi:10.1016/j.matbio.2013.03.005.

[40]   J.L. Li, W.S. Cai, F. Shen, Z. Feng, G.H. Zhu, J. Cao, B. Xu, Protease-activated receptor-2 modulates hepatic stellate cell collagen release and apoptotic status, Arch Biochem Biophys. 545 (2014) 162–166. doi:10.1016/j.abb.2014.01.027.

[41]   S.N. Hartland, F. Murphy, R.L. Aucott, A. Abergel, X. Zhou, J. Waung, N. Patel, C. Bradshaw, J. Collins, D. Mann, R.C. Benyon, J.P. Iredale, Active matrix metalloproteinase-2 promotes apoptosis of hepatic stellate cells via the cleavage of cellular N-cadherin, Liver Int. 29 (2009) 966–978. doi:10.1111/j.1478-3231.2009.02070.x.

[42]   B. Sun, X. Zhang, X. Cheng, Y. Zhang, L. Chen, L. Shi, Z. Liu, H. Qian, M. Wu, Z. Yin, Intratumoral hepatic stellate cells as a poor prognostic marker and a new treatment target for hepatocellular carcinoma, PLoS One. 8 (2013) e80212. doi:10.1371/journal.pone.0080212.

FIGURE LEGENDS

Figure 1: *Expression of miR 23a-5p, miR 28a-5p, miR 199a-3p and miR 29a-3p in Wt and hCOX-2-Tg mice.*

(A) Identification of 16 differentially expressed miRNAs in isolated hepatic stellate cells (HSC) from Wt and hCOX-2-Tg mice, as detected by quantitative real-time PCR (RT-PCR) array. Values are represented in heat map relative to HSC of Wt mice, oil or CCl_4 as appropriate. (B-E) Expression of miR 23a-5p, miR 28a-5p, miR 199a-3p and miR 29a-3p in Wt and hCOX-2-Tg isolated HSC (B), isolated hepatocytes (C), isolated Kupffer cells (D) and total liver (E) analyzed by RT-PCR. miRNA expression was normalized to the average of miR 191-5p, miR 103a-3p and RNU5G RNA expression, and expressed as FI (fold induction) *vs.* Wt CCl_4 defined as 1. Data are means $\pm$ SE of 14-18 (B); 5-7 (C); 4 (D, E) mice per group. *$P<0.05$ *vs*. Wt CCl_4.

Figure 2: *COX-2-dependent PGs regulate the expression of miR 23a-5p and miR 28a-5p in HSC.*

(A, B, C) Validation of the downregulated expression of miR 23a-5p and miR 28a-5p by PGE_2 in primary HSC (A), LX-2 cells (B) and GRX cells (C) analyzed by RT-PCR. Cells were treated with 5 µM PGE_2 (overnight) and 2 ng/ml TGFβ1 (6h). * $P <0.05$ *vs.* TGFβ1 treated cells. (D) Representative Western blot (up) showing expression of α-SMA and COL1A1 protein levels. For densitometric analysis, the relative level of Control (Ctrl) expression was defined as 1, and GAPDH served as a loading control. Results are expressed as band ratio. *$P<0.05$ *vs*. Ctrl. #$P<0.05$ *vs*. TGFβ1 treated cells. (E) Expression of miR 23a-5p and miR 28a-5p in primary HSC cells, treated with 5 µM PGE_2, 2 ng/ml

TGFβ1 and 3 µM TRβ-I inhibitor (LY364947). miRNA expression was normalized to the average of miR 191-5p, miR 103a-3p and RNU5G RNA, and expressed as FI *vs*. Ctrl. Data are means $\pm$ SE of three independent experiments. * *P* <0.05 *vs*. Ctrl. # *P* <0.05 *vs*. TGFβ1+PGE$_2$ treated cells.

Figure 3: *miR 23a-5p is differentially expressed in hCOX-2-Tg mice after BDL.*

(A) Representative images of hematoxylin/eosin (H&E), Picro-Sirius Red and Masson's trichromic (MTC) stained liver paraffin-embedded sections from Wt and hCOX-2-Tg mice after bile duct ligation (BDL). Values of Sirius Red are represented in arbitrary units (A.U.). * *P* <0.05 *vs*. Wt Sham. # *P* <0.05 *vs*. Wt BDL. (B) Blood levels of ALT from Wt and hCOX-2-Tg mice after BDL. Values are in units per liter (U/l). * *P* <0.05 *vs*. Wt Sham. (C) Expression of miR 23a-5p and miR 28a-5p in Wt and hCOX-2-Tg after BDL analyzed by RT-PCR. miRNA expression was normalized to the average of miR 191-5p, miR 103a-3p and RNU5G RNA, and expressed as FI (fold induction) vs. Wt BDL defined as 1. Data are means $\pm$ SE (n=3-4 mice per group). * *P* <0.05 *vs*. Wt BDL. (D) Representative immunohistochemistry (IHC) for α-SMA staining (left panel) from Wt and hCOX-2-Tg mice after BDL. Relative values of α-SMA IHC intensity (%) are at right. * *P* <0.05 *vs*. Wt Sham. # *P* <0.05 *vs*. Wt BDL.

Figure 4: *Functional enrichment of miRNA putative gene targets.*

(A) KEGG pathway enrichment. The top most significantly enriched specific terms were plotted against the negative log10 of the *P* value. Number of target genes and total genes for each term are given in parentheses. There is enrichment of terms related to cell death, actin-filament based processes, proliferation and fibrosis. (B). Interactions within the

31

differentially regulated miRNAs and their gene targets were illustrated using Cytoscape. (C) Expression of *Bcl2-l1, Erk1, Atf2, p38, Fn1, Bmp2, Apaf1, Tradd, Cav1* and *Cdh1* RNA in isolated HSC from Wt and hCOX-2-Tg mice treated with CCl_4 (left), and in primary HSC treated with 5 μM PGE_2 and 2 ng/ml TGFβ1 (right), analyzed by RT-PCR. Values are FI *vs.* Wt CCl_4 or TGFβ1 defined as 1. * $P < 0.05$ vs. Wt CCl_4 (left) or vs. TGFβ1 treated cells (right). (D) Expression of *Erk1, Fn1, Bmp2, Cav1* and *Cdh1* RNA in transfected HSC cells, analyzed by RT-PCR. Primary HSC were transfected with pEGP-miR Null, miR 23a-5p or miR 28a-5p for 48h, using Lipofectamine 2000. Values are normalized to 36b4 RNA and expressed as FI *vs.* Null. Data are means $\pm$ SE of 3-5/14-18 mice per group (C left) or $\pm$ SE of three independent experiments (C right, D). * $P < 0.05$ vs. Null.

Figure 5: *Conditioned medium from hCOX-2-Tg mice isolated hepatocytes protects against HSC activation.*

Primary HSC were treated with conditioned medium from Wt and hCOX-2-Tg mice isolated hepatocytes after oil or CCl_4 treatment. (A) Representative images of α-SMA and COL1A1 immunofluorescence. Cells were analyzed by confocal microscopy and the fluorescence intensity was digitalized and measured. Values of the average fluorescence intensity are expressed up right, in arbitrary units (A.U.). (B) Measured levels of PGE_2 in conditioned medium from Wt and hCOX-2-Tg mice isolated hepatocytes after 24 h of culture. (C) Representative Western blot (up) showing expression of Smad 2/3 protein levels. For densitometric analysis, the relative level of Wt oil expression was defined as 1, and GAPDH served as a loading control. Data are expressed as band ratio. Data are

represented as means $\pm$ SE of three independent experiments. * P <0.05 *vs.* Wt oil. # P <0.05 *vs.* Wt CCl$_4$.

Figure 6: *Conditioned medium from hCOX-2-Tg mice isolated hepatocytes induces apoptosis and decreases the proliferation of HSC.*

Primary HSC were treated with conditioned medium from Wt and hCOX-2-Tg mice isolated hepatocytes after oil or CCl$_4$ treatment. (A) Representative images of PCNA and Ki67 immunofluorescence. Cells were analyzed by confocal microscopy and the fluorescence intensity was digitalized and measured. Values of the average fluorescence intensity are expressed in arbitrary units (A.U.). (B) MTT experiment represented in percentage (Wt oil is 100). (C) Representative images of caspase-3 immunofluorescence. Values of the average fluorescence intensity are expressed in arbitrary units (A.U.). (D) Representative Western blot showing expression of caspase-3 and BAX protein levels. For densitometric analysis, the relative level of Wt oil expression was defined as 1, and GAPDH served as a loading control. Data are expressed as band ratio. Data are means $\pm$ SE of three independent experiments. * P <0.05 *vs.* Wt oil. # P <0.05 *vs.* Wt CCl$_4$.

Figure 7: *miR 23a-5p and miR 28a-5p induce fibrosis and decrease apoptosis in transfected HSC.*

Primary HSC were transfected with pEGP-miR Null, miR 23a-5p or miR 28a-5p for 48h, using Lipofectamine 2000. (A) Representative Western blot of α-SMA and COL1A1. * P <0.05 *vs.* Null. (B, C, D) Cells were treated with 5 μM PGE$_2$ and 2 ng/ml TGFβ1, in addition to transfection. (B) Representative Western blot of α-SMA, COL1A1, ERK, CDH1 and BMP2. (C) MTT experiment relative to Null (100). (D) Representative Western

blot of caspase 3 cleaved and Bcl-xL. For densitometric analysis, the relative level of Null was defined as 1, and GAPDH served as a loading control. Data are expressed as band ratio. Data are means $\pm$ SE of three independent experiments. * P <0.05 *vs.* TGFβ1+Null; # P <0.05 *vs.* TGFβ1+PGE$_2$+Null.

Figure 8: *Synthesis of PGE$_2$ in hepatocytes protects against fibrosis.*

In the presence of PGE$_2$, the apoptosis of the hepatocytes decreases and, therefore, the apoptotic body engulfment by the HSCs, thus reducing its activation. Moreover, PGE$_2$ downregulates miR-23a and miR-28a expression in HSCs, resulting in an increase of ERK, BMP2, CAV1 and CDH1 levels. This leads to an increment in apoptosis together with an inhibition of HSC proliferation. As a consequence, a decrease of α-SMA and COL1A1 is shown in HSC.

Figure 1
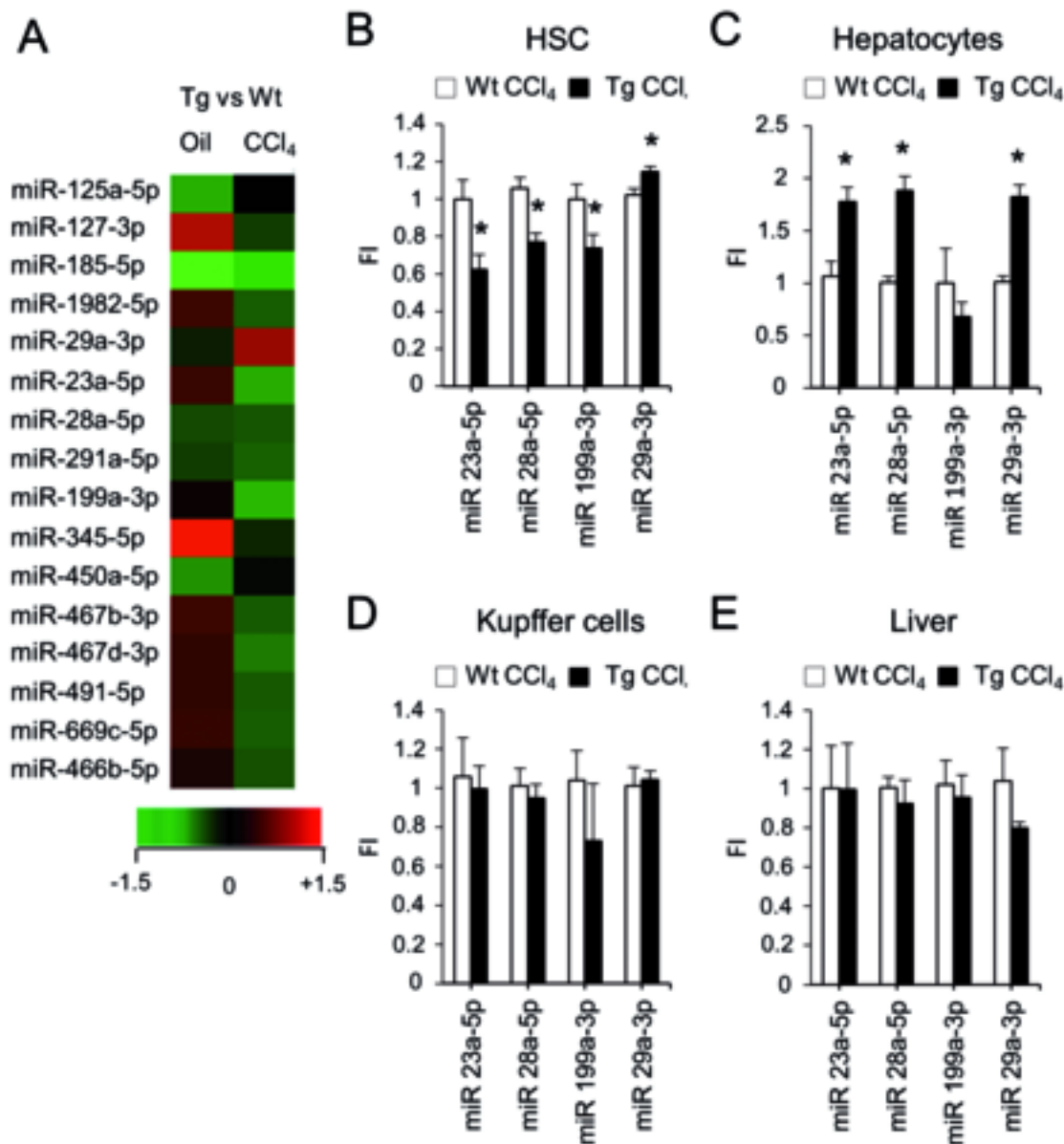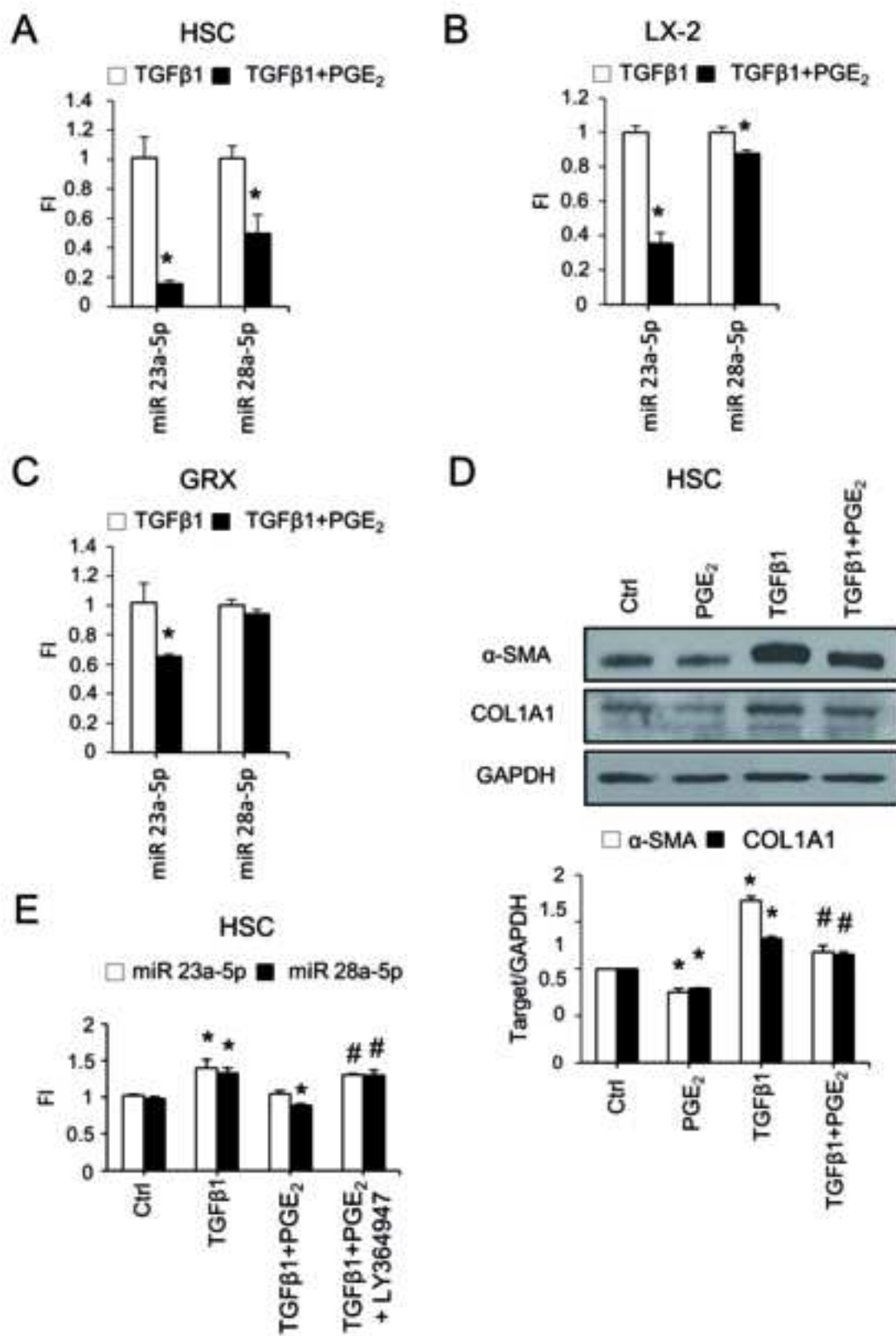
A

Tg vs Wt

Oil   CCl₄

miR-125a-5p
miR-127-3p
miR-185-5p
miR-1982-5p
miR-29a-3p
miR-23a-5p
miR-28a-5p
miR-291a-5p
miR-199a-3p
miR-345-5p
miR-450a-5p
miR-467b-3p
miR-467d-3p
miR-491-5p
miR-669c-5p
miR-466b-5p

-1.5   0   +1.5

Figure 2

Figure 3

Figure 4

A

Pathways in cancer (277/324)
MAPK signaling pathway (141/268)
Wnt signaling pathway 8105/150)
Focal adhesion (112/197)
Apoptosis (53/85)
mTOR signaling pathway (29/52)
TGF beta signaling pathway (47/87)
ECM receptor interaction(49/82)
p53 signaling pathway (36/69)
Cell cycle (66/128)

-lg (Pvalue)

B

FN1, p38, miR-199a, CAV1, miR-23a, CDH1, FASL, miR-29a, TRADD, ERK1, miR-28a, BMP2, BCL2L1

C

HSC — ☐ Wt CCl$_4$ ■ Tg CCl$_4$

HSC — ☐ TGFβ1 ■ TGFβ1+PGE$_2$

Bcl2-l1, Erk1, Atf2, p38, Fn1, Bmp2, Apaf1, Tradd, Cav1, Cdh1

D

HSC — ☐ Null ■ miR 23a-5p ☐ miR 28a-5p

Erk1, Fn1, Bmp2, Cav1, Cdh1

Figure 5

A

B

C
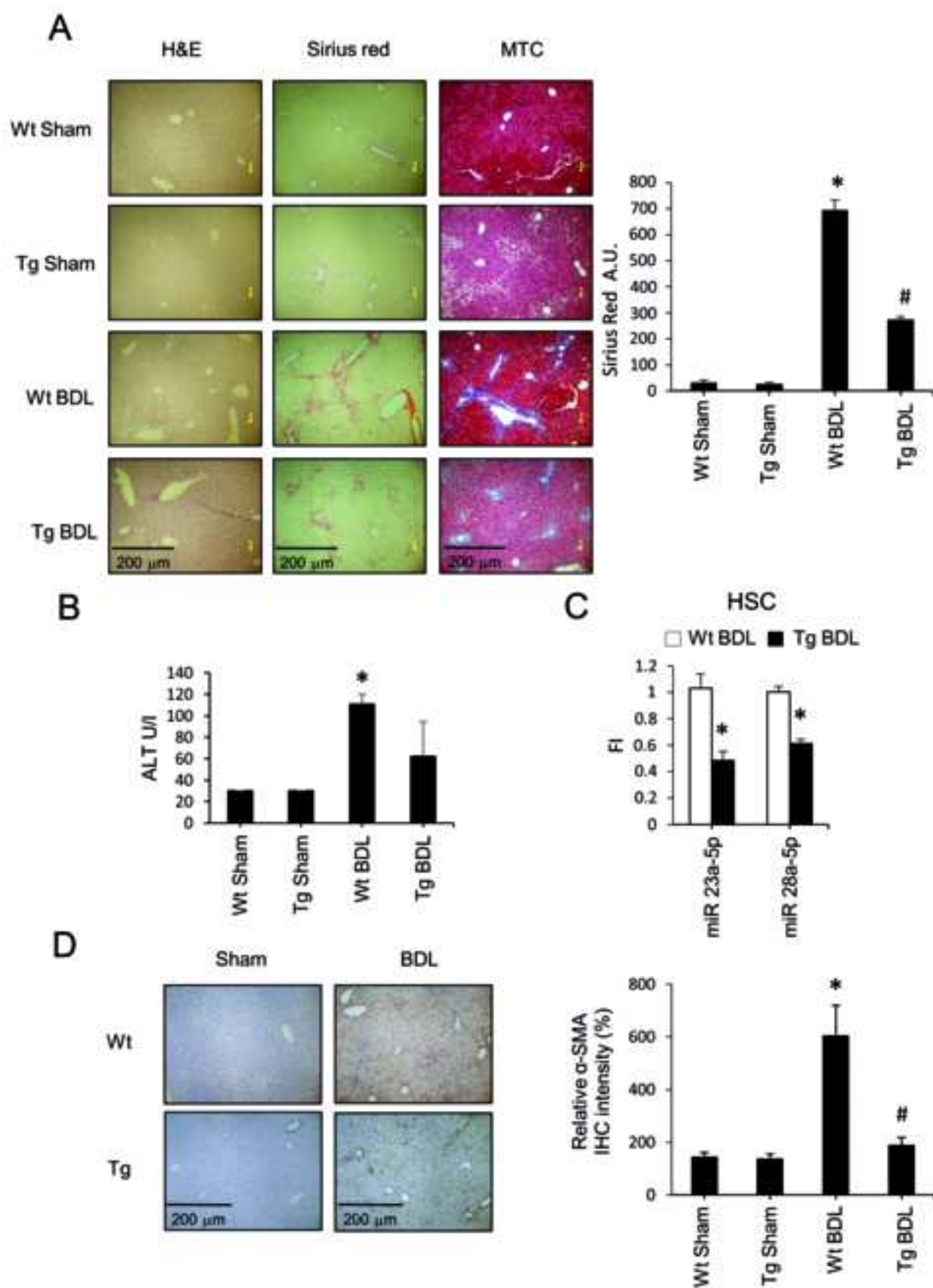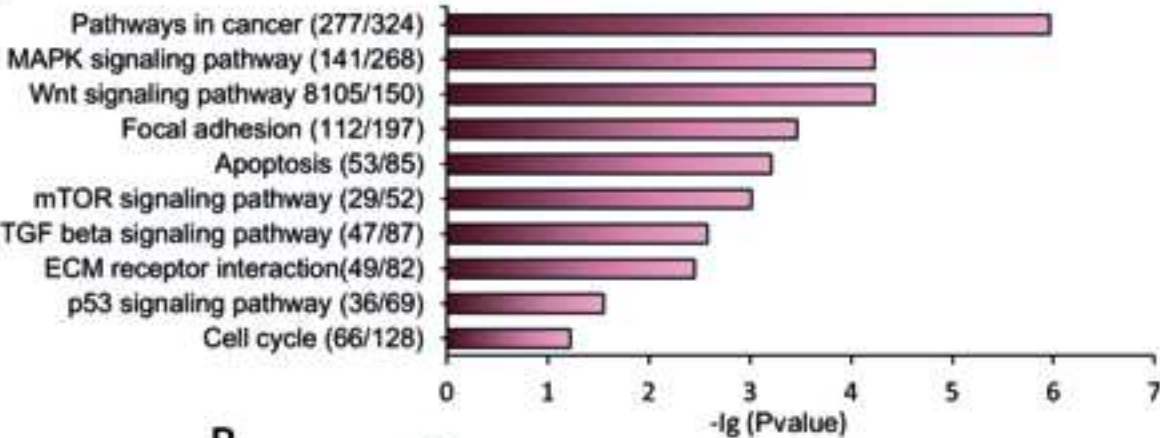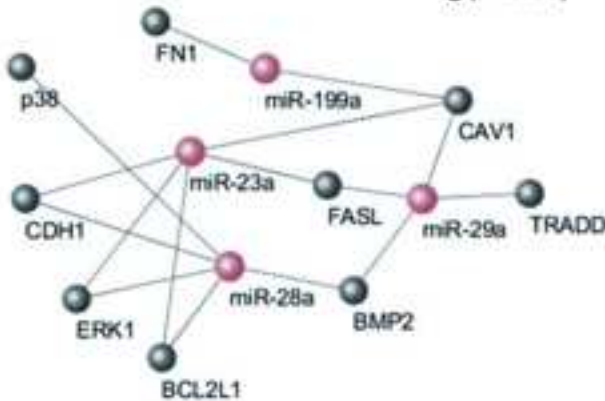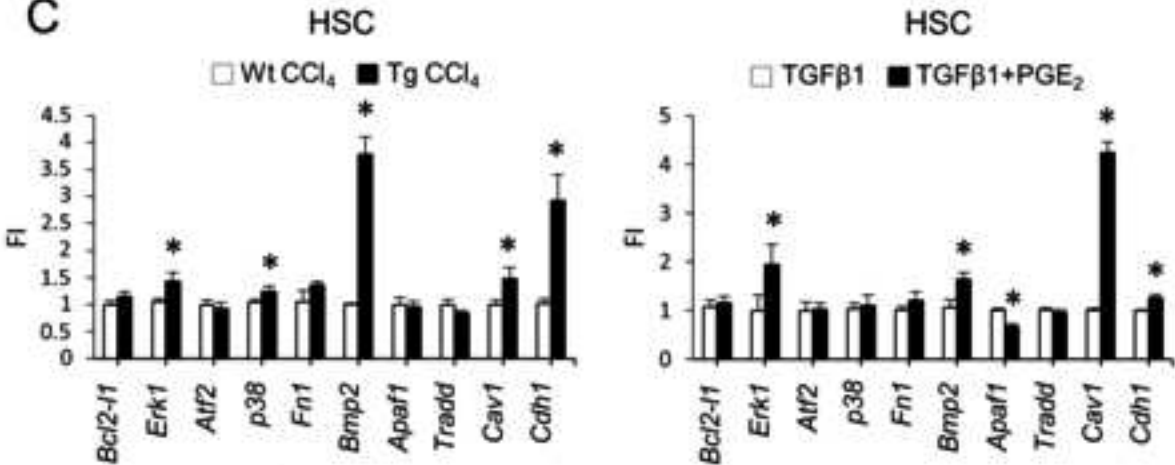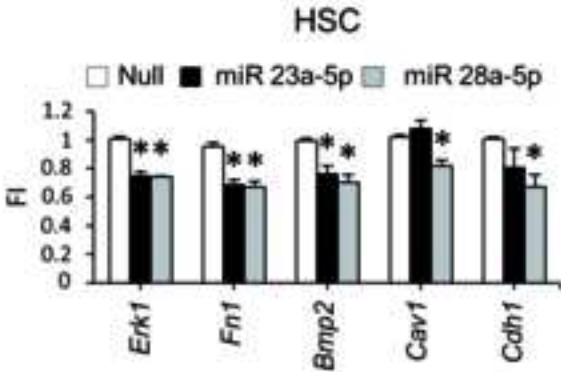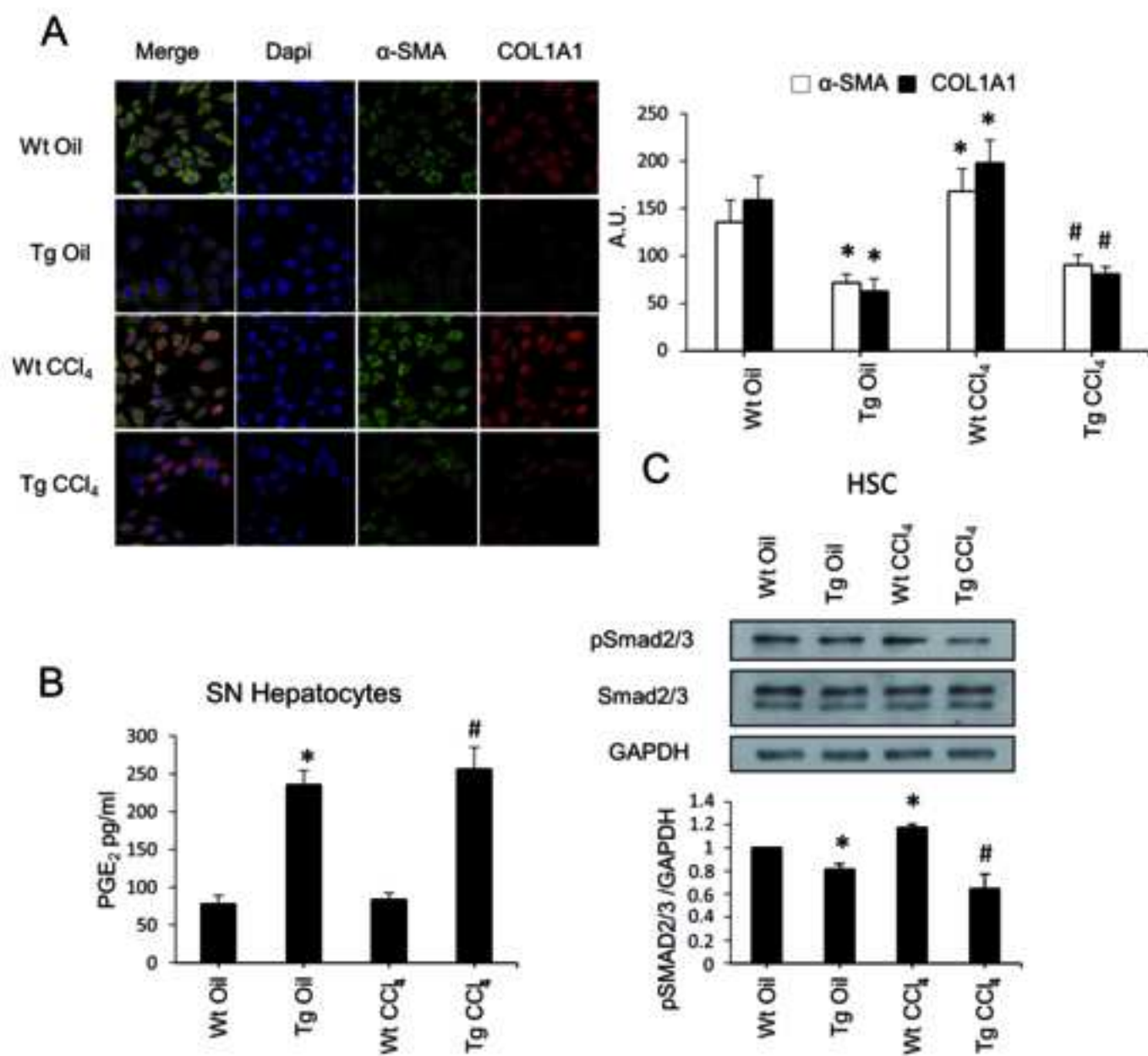
Figure 6
Click here to download high resolution image

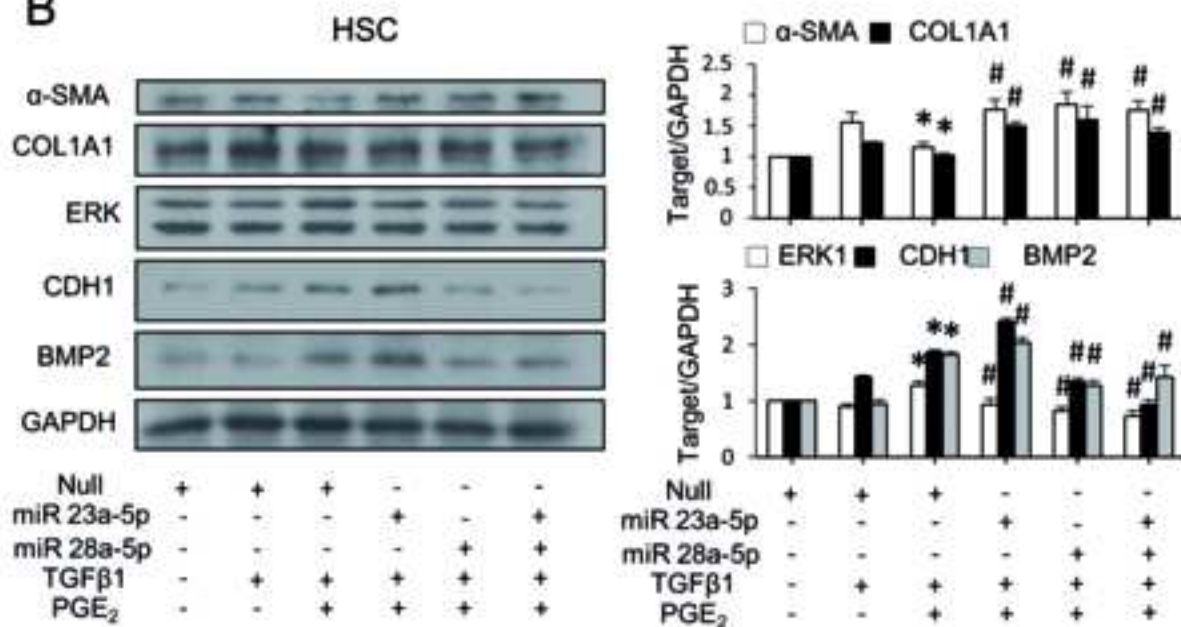Figure 6

Figure 7

A

B

HSC

C

HSC

D

HSC
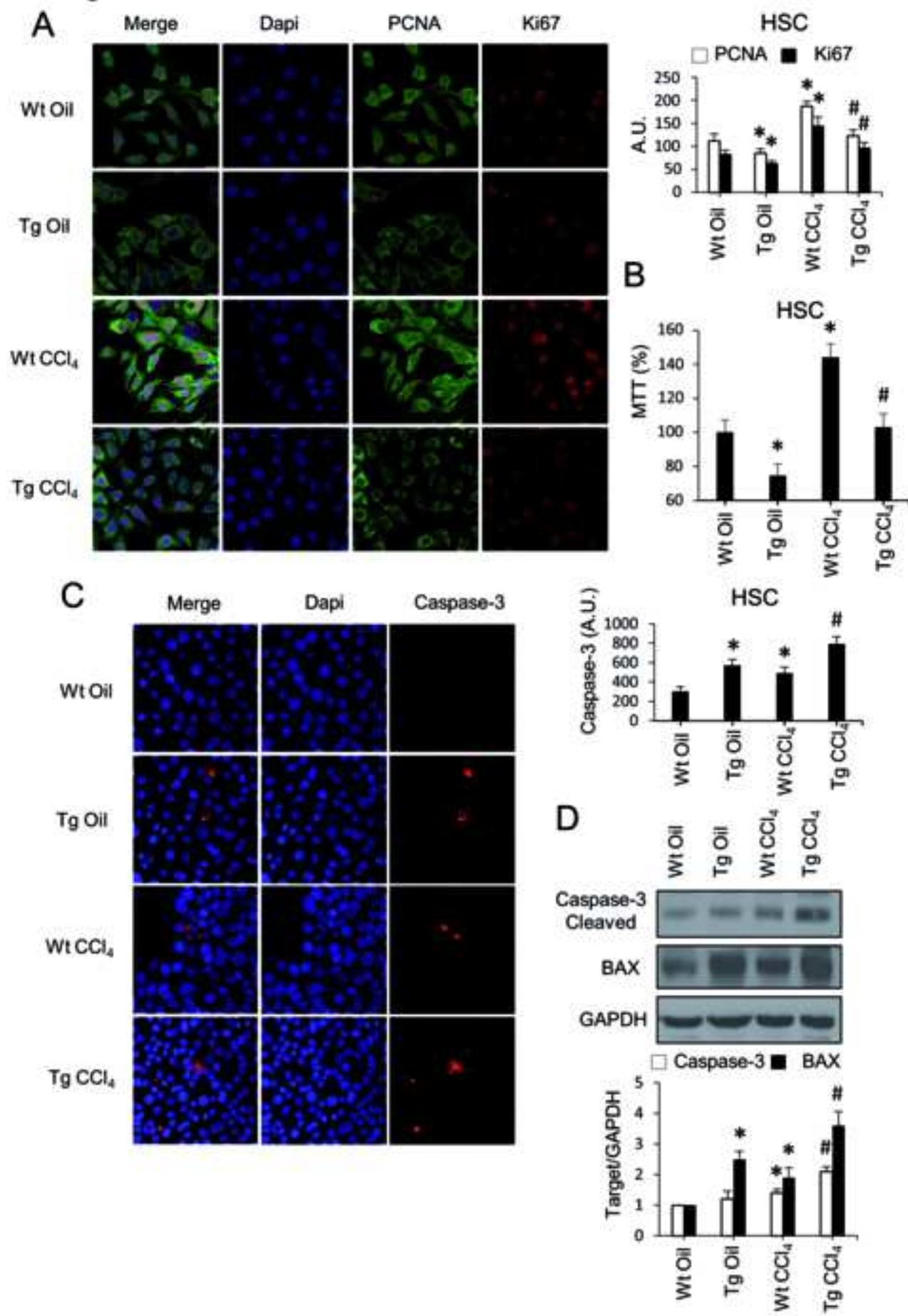
Figure 8
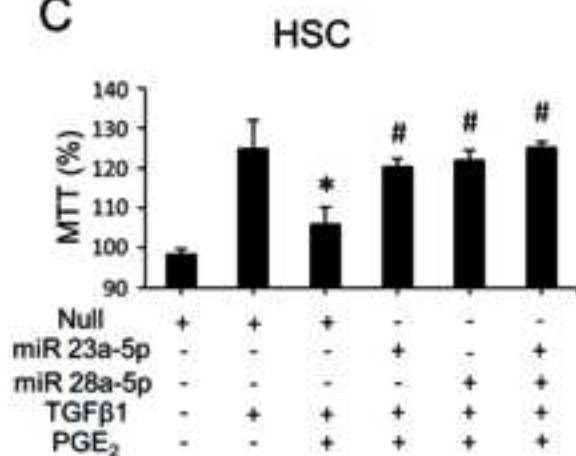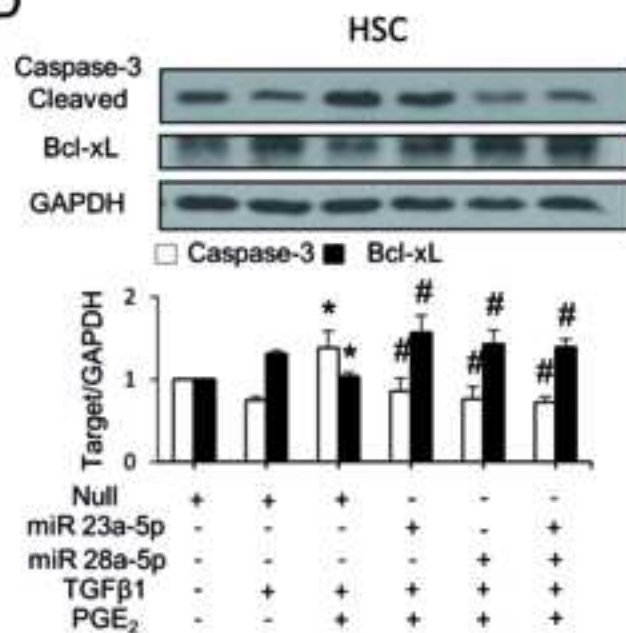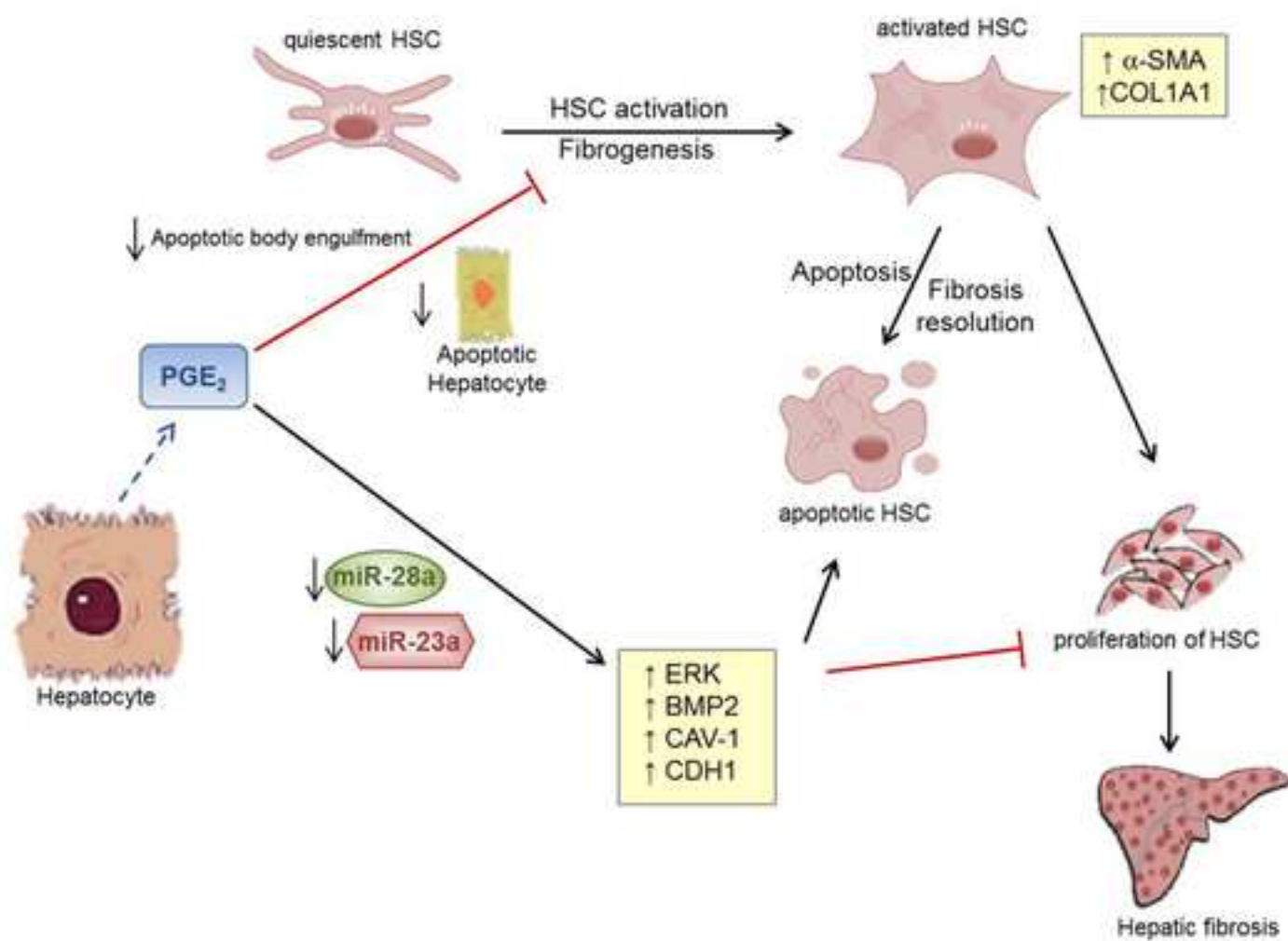**Click here to download high resolution image**
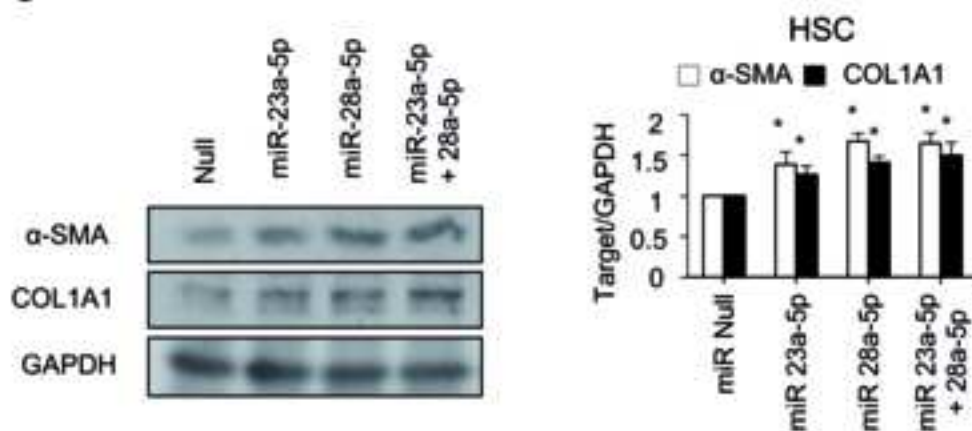
Figure 8

SUPPLEMENTARY MATERIAL

Chemicals

Antibodies were from Santa Cruz Biotechnology (Dallas, TX, USA), Sigma-Aldrich (St. Louis, MO, USA), Cell Signaling Technology (Danvers, MA, USA), Abcam (Cambridge, United Kingdom), Calbiochem/Merck Millipore (Billerica, Massachusetts, USA), Ambion/Thermo Fisher Scientific (Waltham, Massachusetts, USA) and BD Biosciences (Franklin Lakes, NJ, USA). Reagents were from Merck (Kenilworth, New Jersey, United States), Roche Diagnostics (Indianapolis, Indiana, United States), Cayman Chemical (Ann Arbor, Michigan, USA) or Sigma-Aldrich. Reagents for electrophoresis were obtained from Bio-Rad (Hercules, CA, USA). Tissue culture dishes were from Falcon (Becton Dickinson Labware, Franklin Lakes, NJ, USA). Tissue culture media were from Gibco (Life Technologies™, Carlsbad, CA, USA).

Human Subjects

This study comprised serum from 25 patients with a clinical diagnosis of NAFLD who underwent a liver biopsy with diagnostic purposes. Inclusion criteria for NAFLD patients were based on an alcohol intake lesser than 20 g/day, the presence of biopsy-proven steatosis with/without necroinflammation and/or fibrosis, and no evidence of hepatitis B and/or C virus (HBV and/or HCV, respectively) infection as well as human immunodeficiency virus (HIV) infection. We further studied 13 patients with asymptomatic cholelithiasis to whom a liver biopsy was taken during programmed laparoscopic cholecystectomy. All had histologically normal liver (NL). The study was performed in agreement with the 1975 Declaration of Helsinki, and with local and national laws. The Human Ethics Committee of Santa Cristina University Hospital approved the study procedures, and written informed consent was obtained from all patients before inclusion in the study.

Human subjects histopathological evaluation

Hematoxylin-eosin and Masson´s trichrome-stained paraffin-embedded liver biopsy sections were examined and interpreted by the same experienced hepatopathologist (C G-M), who was unaware of the clinical data. Kleiner´s histological scoring system (1) was used to evaluate the degree of hepatocyte ballooning and lobular inflammation as well as the stage of fibrosis.

The miRNA serum analysis was performed by IRYCIS Core Facility miRNAs-based Biomarkers and Therapeutic Targets from the Service of Pathological Anatomy of the Ramón y Cajal Hospital.

Animal Histopathology assessment

Hematoxylin-Eosin (H&E) and Masson´s trichrome-stained (MTC) paraffin-embedded liver biopsy sections from studied mice were evaluated by the same experienced liver pathologist (J.V-C) blinded to the features of animal groups. The fibrosis stage was assessed using the NAFLD scoring system for mice models validated by Liang *et al*., (2). Fibrosis staging was defined as 0, none; 1, perisinusoidal and/or pericentral; 2, incomplete central/central bridging fibrosis; 3, complete central/central bridging fibrosis; and 4, definite cirrhosis.

Quantitative analysis of collagen in Sirius Red-stained liver sections was performed using imaging analysis software (ImageJ software (http://imagej.nih.gov)). Briefly, paraffin sections of 20 μm thickness were stained in 0.1% Sirius red in saturated picric acid. The red-stained area (μm^2) was measured in five consecutive fields (40X). Fibrotic area percentage was calculated relative to the total area examined.

Immunohistochemistry of α-SMA

The liver tissue sections (5 μm) were dewaxed, hydrated and subjected to heat-induced antigen retrieval. Sections were blocked and incubated overnight at 4 °C with mouse

anti-alpha-smooth muscle actin (α-SMA) antibody (Sigma-Aldrich, St. Louis, MO) at 1:300 dilution. Negative-control antibodies consisted of species-matched, and where appropriate, IgG subclass-matched Ig, used at the same dilution. The sections were subsequently washed and incubated with HRP-conjugated goat anti-mouse IgG secondary antibodies, followed by incubation for 5 min with 3,3′-diaminobenzidine tetrachloride and visualization of specific staining under light microscopy. Stained slides were analyzed by light microscopy, and high-power field images (magnification × 100) of the livers were taken of each mouse (Axiophot Zeiss; Germany). α-SMA deposition was evaluated semi-quantitatively according to the intensity of staining using plugins Fiji for Image J.

Isolation and culture of hepatocytes

Hepatocytes were isolated from non-fasting male Wt and hCOX-2-Tg mice by perfusion through the inferior cava vein with Hank's balanced salt solution (HBSS) (Gibco), 10 mM HEPES pH 7.4, 0.2 mM EGTA, 500U heparin and William's E medium (Sigma) with 0.56 mg/ml (in oil/Sham mice) or 0,8 mg/ml (in CCl_4/BDL mice) collagenase type 1 (C5138-1G, Sigma). After filtering through a cell strainer (100 μm) and centrifugation at 500 rpm, 4ºC for 5 min, cells were resuspended in the following attachment culture medium (AM): DMEM/F12 (1:1), 20 mM HEPES pH 7.4, 0.05% $NaHCO_3$, 6 mM glucose, 10% FBS (Sigma), 5 mg/ml BSA, 100 U/ml penicillin, 100 μg/ml streptomycin and 50 μg/ml gentamicin, and purified by density gradient centrifugation (1000 rpm, 4ºC for 10 min) using a isotonic solution of Percoll (GE Healthcare Bio-Sciences AB, Uppsala, Sweden), 150 mM NaCl and 1X HBSS. Finally, after washing the cells 2-3 times with AM (500 rpm, 4ºC for 5 min), cells were resuspended directly in 700 μl QIAzol Lysis Reagent (Qiagen, Valencia, CA) for further mRNA analysis or were plated in 6 multiwell dishes at a density of 500,000 cells/well

in attachment culture medium with 10% FBS. Cell viability was checked by Trypan blue exclusion. The cell supernatant (hepatocyte conditioned medium) was obtained after 6, 18 and 24h of culture and stored at -80ºC for further analysis.

Isolation of kupffer cells

For Kupffer cells (KC) isolation, the supernatant from the first centrifugation of the hepatocyte isolation protocol was collected and centrifuged at 500 rpm for 5 min at 4ºC to discard the pellet with remaining hepatocytes, as described previously (3). Briefly, the latest supernatant was centrifuged at 1500 rpm for 10 min at 4ºC and the pellet containing the KC was resuspended in the attachment culture medium. Cells were mixed by inversion with 50% Percoll in 1X HBSS and centrifuged at 2300 rpm for 30 min without acceleration or brake at room temperature. Finally, KC pellet was washed with PBS, centrifuged twice at 1500 rpm for 10 min at 4ºC to wash out the residual Percoll solution and cells were resuspended directly in 700 μl QIAzol Lysis Reagent (Qiagen) for further mRNA analysis.

Hepatic stellate cell lines cultures

The LX-2 cell line, a spontaneously immortalized human hepatic stellate cell, was purchased from Millipore, Billerica, MA, SCC064. GRX is a mouse myofibroblast hepatic stellate cell line purchased from Rio de Janeiro Cell Bank BCRJ 0094. Both were recently authenticated using Promega's StemElite [TM] ID System in the Genomics Core facility of the IIB. LX-2 cells were maintained in EmbryoMAX medium (Millipore, Billerica, MA, USA) supplemented with glutamine and 2% fetal bovine serum (FBS) (Sigma). GRX cells were maintained in Dulbecco's culture medium (DMEM) (Gibco), supplemented with 5% FBS. Primary HSC isolated from Wt mice were used too, maintained in Dulbecco's culture medium (DMEM) (Gibco), supplemented with 10% FBS. All of them were cultured in a humidified atmosphere

with 5% CO_2 at 37ºC. For the experiments, cells were seeded into six ($4x10^5$/well for

LX-2 and GRX; $1,5x10^5$/well for primary HSC) or twelve ($15x10^4$/well for LX-2 and

GRX; $6x10^4$/well for primary HSC)-well culture plates, serum starved and treated with

5 μM PGE_2 (overnight), 2 ng/ml TGF-β1 (6h) and 3 μM TRβ-I inhibitor (LY364947)

(1h). Also, primary HSC were treated for 24h with hepatocyte conditioned medium

from Wt and hCOX-2-Tg mice isolated hepatocytes after oil or CCl_4 treatment.

RNA extraction and quantitative real-time PCR analysis

Total RNA and miRNA from liver and cell samples was extracted by using 700 μl

QIAzol Lysis Reagent and purified with a miRNeasy Mini Kit (Qiagen).

RNA (250 ng in 20 μl) was reverse transcribed using a High Capacity cDNA Reverse

Transcription Kit following the manufacturer's indications (Applied Biosystems, Foster

City, California, United States). cDNA was used as a template for RT-PCR with Power

SYBR Green Master Mix (Applied Biosystems). RT-PCR was performed with a

7900HT Fast-Real Time PCR System (Life Technologies) with the forward and reverse

primers described in Table I. Specific primers were purchased from Invitrogen. PCR

thermocycling parameters were 95°C for 10 min, 40 cycles of 95°C for 15 s and 60°C

for 1 min; followed by a dissociation curve consisting of 95ºC for 15 s; 60ºC for 15 s;

95ºC for 15 s. Each sample was run in triplicate and was normalized to 36b4 mRNA.

The replicates were then averaged, and fold induction (FI) was determined in a ΔΔCt

based fold-change calculations.

For quantification of mature miRNAs, RNA (155 ng in 10 μl) was polyadenylated and

reverse transcribed to cDNA using a Universal cDNA Synthesis Kit II (Part from

miRCURY LNA[TM] Universal RT microRNA PCR, Exiqon). cDNA was used as the

template for RT-PCR ExiLENT SYBR® Green master mix (Exiqon) with the

microRNA LNA[TM] PCR primers set (Exiqon, see Table II). RT-PCR was performed

with a 7900HT Fast-Real Time PCR System (Life Technologies), and the thermocycling parameters were 95°C for 10 min and 40 cycles of 95°C for 10 s and 60°C for 1 min; followed by a dissociation curve consisting of 95ºC for 15 s; 60ºC for 15 s; 95ºC for 15 s. Each sample was run in triplicate and was normalized to the average value of hsa-miR-191-5p, has-miR-103a-3p and RNU5G (LNA^{TM} PCR primers set, Exiqon). Melting curve analysis was performed to confirm the specificity of the PCR products. The replicates were then averaged, and FI was determined in a ΔΔCt based fold-change calculations.

Construction and transfection of miRNA vectors

Precursors for mmu-miR-23a, and mmu-miR-28a were generated in green fluorescent protein (GFP)-puromycin (pEGP)-miR cloning vector (Cell Biolabs, San Diego, CA). Briefly, microRNA stem-loop sequences were identified using the Sanger Center miRNA database (http://microrna.sanger.ac.uk/sequences) and were amplified by PCR from genomic DNA. PCR products were cloned into the BamHI-NheI restriction site of pEGP-miR vector, and the correct orientation and integrity of the construct were confirmed by sequencing.

For transfection experiments, primary HSC were seeded into six ($16x10^4$/well) or twelve ($6x10^4$/well)-well culture plates at 70% confluence. After 24 h, cells were starved for 4h, and then transfected with 4 μg (6 well) or 1.6 μg (12 well) of pEGP-miR, using Lipofectamine 2000, in DMEM without FBS supplemented with 0.2% Bovine Serum Albumin (BSA). After 16 h of incubation at 37°C, transfection medium was replaced with 2 ml (6 well) or 1.5 ml (12 well) of complete medium without FBS. After 48 h from transfection, cells were collected for Western blot and RT-PCR analyses.

In order to determine the efficiency of transfection, cells were observed in a fluorescence microscope to view GFP fluorescence. Transfection rate was determined using ImageJ software (http://imagej.nih.gov) and expressed in %.

Determination of metabolites and MTT assay

PGE_2 was determined in hepatocyte conditioned medium from Wt and hCOX-2-Tg mice isolated hepatocytes after oil or CCl_4 treatment, and patient´s serum by specific immunoassay (DetectX Prostaglandin E_2 Enzyme Immunoassay Kit; Arbor Assays, Ann Arbor, MI, USA). Serum ALT activity was determined using Reflotron strips (Roche Diagnostics, Barcelona, Spain), accordingly with the manufacturer's instructions.

For MTT (Thiazol Blue Tetrazolium Blue) assays, cells were seeded into 96 well culture plates ($8x10^3$/well). After adding the corresponding stimuli, cells were washed with 1X PBS and added 100 µl of complete medium. 20 µl of 2 mg/ml MTT was added, and cells were incubated 4h at 37ºC without light. After that time, 100 µl DMSO was added, and absorbance was measured at 570 and 630 nm.

Immunofluorescence assays

Primary HSC cells ($5x10^3$) were cultured in Culture Slides (Falcon, Ref. 354108). After adding the corresponding stimuli, the cells were washed with 1X PBS and fixed for 10 min with 2% paraformaldehyde at room temperature, washed with 1X PBS, and permeabilized with 0.1% Triton X-100 in 1X PBS for 3 min at room temperature. After blocking with 2% bovine serum albumin (BSA) for 30 min at room temperature, the cells were incubated at 4ºC overnight with the corresponding primary antibodies diluted 1:500 in 1X PBS 2% BSA. The next day, cells were washed several times and incubated with fluorochrome-conjugated secondary antibodies (Invitrogen) for 1h at room temperature without light (diluted 1/500 in 1X PBS 2% BSA). Then cells were treated

with 4', 6-diamidino-2-phenylindole (DAPI, diluted 1/1000 in 1X PBS 2% BSA) for 20 min at room temperature. The culture slides were dismantled, in order to leave micro-scope slides. The glass coverslips were mounting with Prolong (Thermo Fisher Scientific) on those micro-scope slides. After 24h, the image was acquired in a fluorescence Confocal Leica TCS SP5 X.

Cell cycle analysis

Primary HSC were treated for 24h with hepatocyte conditioned medium from Wt and hCOX-2-Tg mice isolated hepatocytes after oil or CCl_4 treatment. After that, cell supernatant was collected together with the cells. Cells were washed in 1X PBS, centrifuged at 1200 rpm, 5 min, and then fixed with 700 μl 70% ice-cold ethanol at 4ºC 1h in agitation. The cells were then centrifuged and resuspended in 1X PBS for 3 times, to remove ethanol residues. Finally, cells were resuspended in 200 μl 1X PBS, containing 0.02 μg/μl propidium iodide and 0.1 μg/μl RNase A for 1h in agitation and darkness. Flow cytometry analysis was performed using Cytomics FC500.

Western blot analysis

Extracts from cells ($2–3\times10^6$) were obtained as previously described (5). The protein extract was obtained through centrifugation at 12000 rpm at 4°C for 15 min. Finally, the total protein levels on the supernatant were measured using the Bradford reagent (Bio-Rad) (6). For Western blot analysis, whole-cell extracts were boiled for 5 min in Laemmli sample buffer, and equal amounts of protein (20–40 μg) were separated by 8–15% SDS-polyacrylamide electrophoresis gel (SDS-PAGE). The relative amounts of each protein were determined with the polyclonal or monoclonal antibodies described in Table III. After incubation with the corresponding anti-rabbit, anti-goat or anti-mouse horseradish peroxidase conjugated secondary antibody, blots were developed by the ECL protocol (GE Healthcare Life Sciences, Pittsburgh, PA, USA). Target protein band

8

densities were normalized with GAPDH. The blots were revealed using Medical X-Ray Film Blue (Agfa-Gevaert, Mortsel, Belgium) and different exposition times were performed for each blot to ensure the linearity of the band intensities. Densitometric analysis of the bands was carried out using ImageJ software (http://imagej.nih.gov) and expressed in arbitrary units.

REFERENCES

1. Kleiner DE, Brunt EM, Van Natta M, Behling C, Contos MJ, Cummings OW, et al. Design and validation of a histological scoring system for nonalcoholic fatty liver disease. Hepatology 2005;41:1313–1321.

2. Liang W, Menke AL, Driessen A, Koek GH, Lindeman JH, Stoop R, et al. Establishment of a general NAFLD scoring system for rodent models and comparison to human liver pathology. PLoS One 2014;9:e115922.

3. Pardo V, Gonzalez-Rodriguez A, Guijas C, Balsinde J, Valverde AM. Opposite cross-talk by oleate and palmitate on insulin signaling in hepatocytes through macrophage activation. J Biol Chem 2015;290:11663–11677.

4. Mederacke I, Dapito DH, Affo S, Uchinami H, Schwabe RF. High-yield and high-purity isolation of hepatic stellate cells from normal and fibrotic mouse livers. Nat Protoc 2015;10:305–315.

5. Casado M, Mollá B, Roy R, Fernández-Martínez A, Cucarella C, Mayoral R, et al. Protection against Fas-induced liver apoptosis in transgenic mice expressing cyclooxygenase 2 in hepatocytes. Hepatology 2007;45:631–638.

6. Bradford MM. A rapid and sensitive method for the quantitation of microgram quantities of protein utilizing the principle of protein-dye binding. Anal. Biochem 1976;72:248–254.

SUPPLEMENTARY TABLE I: The oligonucleotide sequences

Gene	Orientation	Primer sequence 5´->3´
m-Bcl2-l1	Forward	AGGCGATGAGTTTGAACTGC
	Reverse	TGAAGCTGGGATGTTAGATCACT
m-Erk1 *(MAPK3)*	Forward	ACCACATTCTAGGTATCTTGGGT
	Reverse	AGTTTCGGGCCTTCATGTTAAT
m-Atf2	Forward	CCGTTGCTATTCCTGCATCAA
	Reverse	TTGCTTCTGACTGGACTGGTT
m-p38 *(MAPK14)*	Forward	GACCTTCTCATAGATGAGTGGAAGA
	Reverse	CAGGACTCCATTTCTTCTTGGT
m-Fn1	Forward	GCTCAGCAAATCGTGCAGC
	Reverse	CTAGGTAGGTCCGTTCCCACT
m-Bmp2	Forward	GGGACCCGCTGTCTTCTAGT
	Reverse	TCAACTCAAATTCGCTGAGGAC
m-Apaf1	Forward	AGTAATGGGTCCTAAGCATGTTG
	Reverse	GCGATTGGGAAAATCACGTAAAA
m-Tradd	Forward	AGCCATACAGGTAGCTTCTGC
	Reverse	GTGGCCGGTTCACTACGAG
m-Cav1	Forward	AGCCCAACAACAAGGCCAT
	Reverse	GCAATCACATCTTCAAAGTCAATCTT
m-Cdh1	Forward	TCGGAAGACTCCCGATTCAAA
	Reverse	CGGACGAGGAAACTGGTCTC
m-α-sma	Forward	CCCAGACATCAGGGAGTAATGG
	Reverse	TCTATCGGATACTTCAGCGTCA
m-Col1a1	Forward	AATGGCACGGCTGTGTGCGA
	Reverse	AGCACTCGCCCTCCCGTCTT

SUPPLEMENTARY TABLE II: LNA^{TM} PCR primers set (Exiqon)

Gene	Reference
hsa-miR-23a-5p	205631
hsa-miR-28-5p	204322
hsa-miR-199a-3p	204536
hsa-miR-29a-3p	204698
hsa-miR-191-5p	204306
hsa-miR-103a-3p	204063
RNU5G	203908

SUPPLEMENTARY TABLE III: Primary antibodies

| Detects	Comercial house	Reference
α-SMA	Sigma-Aldrich	A5228
COL1A1	Calbiochem	234167
GAPDH	Ambion	AM4300
pSMAD2/3	Santa Cruz Biotechnology	sc11769
SMAD2/3	Santa Cruz Biotechnology	sc6033
PCNA	Santa Cruz Biotechnology	sc56
Ki67	Abcam	ab15580-100
Caspase 3 cleaved	Cell Signaling	9661
BAX	Cell Signaling	2772
pERK	Cell Signaling	9101
ERK	Cell Signaling	9102
Bcl-xL	Cell Signaling	2762S
BMP2	Abcam	ab6285
E-Cadherin	BD Biosciences	610181

SUPPLEMENTARY FIGURE LEGENDS

Supplementary Figure 1: *hCOX-2 Tg mice are protected against fibrosis.* (A) Representative images of hematoxylin/eosin (H&E) and Picro-Sirius Red stained liver paraffin-embedded sections from Wt and hCOX-2-Tg mice after 9 weeks of CCl_4 treatment. (B) Values of collagen area from Sirius Red are represented. (C) Blood levels of ALT in Wt and hCOX-2-Tg mice treated with or without CCl_4 (U/l). Data are means $\pm$ SE (n=12-23 animals per group). (D) Expression of *α-Sma* and *Col1a1* RNA in culture HSC cells from Wt and hCOX-2-Tg mice treated with or without CCl_4, analyzed by RT-PCR. Values are normalized to 36b4 RNA and expressed as FI (fold induction) *vs.* Wt oil. Data are means $\pm$ SE of three independent experiments. (E) Representative Western blot showing α-SMA in HSC from Wt and hCOX-2-Tg mice treated with or without CCl_4. For densitometric analysis, the relative level of Wt CCl_4 expression was defined as 1, and GAPDH served as a loading control. Results are expressed as band ratio. Data are means $\pm$ SE of three independent experiments. * $P < 0.05$ *vs.* Wt Oil, # $P <0.05$ *vs.* Wt CCl_4.

Supplementary Figure 2: *Cellular cycle profile in HSC.* Primary HSCs were treated with conditioned medium from Wt and hCOX-2-Tg mice isolated hepatocytes after oil or CCl_4 treatment. Representative cellular cycle profile, measured by flow cytometry. Values are the percentage of cells at each phase.

Supplementary Figure 3: *Transfection rate of miRNAs in HSC.* Primary HSCs were transfected with pEGP-miR Null, miR 23a-5p or miR 28a-5p for 48h, using Lipofectamine 2000. (A) Representative images of GFP fluorescence. Values of transfection rate (%) are shown. (B) Expression of miR 23a-5p and miR 28a-5p in HSC, analyzed by RT-PCR. miRNA expression was normalized to the average of miR 191-5p, miR 103a-3p and RNU5G RNA, and expressed as FI (fold induction) *vs.* Null.. Data are means $\pm$ SE of three independent experiments. * $P <0.05$ *vs.* pEGP-miR Null.

Supplementary Figure 4: *PGE_2 increases and correlates inversely to miR 28-5p in human fibrosis serum specimens.* (A) PGE_2 concentration was determined in different fibrosis score samples. * $P<0.01$ vs. NL (normal liver, fibrosis score 0 samples). (B) The expression of miR 23a-5p and miR 28-5p was analyzed using RT-PCR. Data were normalized to UniSp2 RNA levels and expressed as FI *vs.* NL. * $P < 0.05$ vs. NL (C) The correlation between PGE_2 and miR 28-5p expression is shown. The coefficient of determination (R^2) and Pearson´s correlation coefficient (*p*) was calculated.
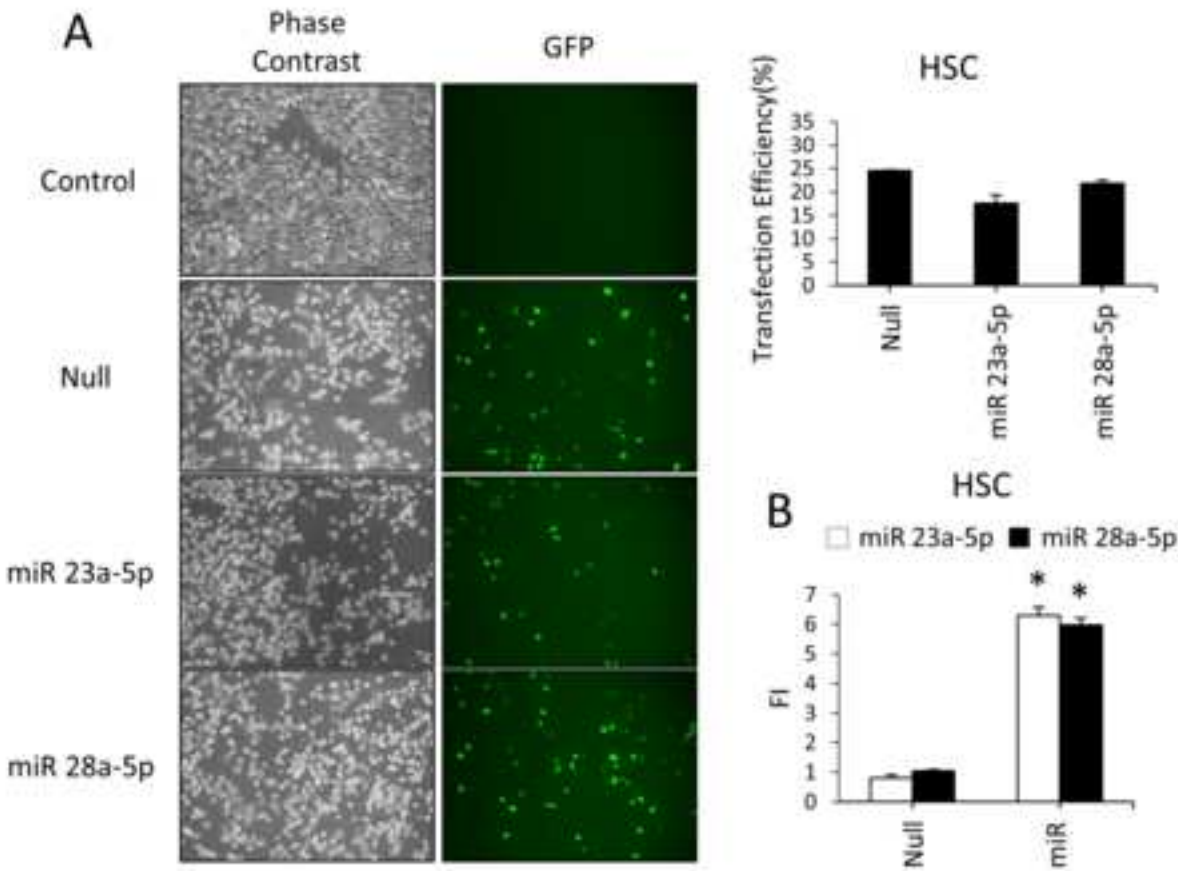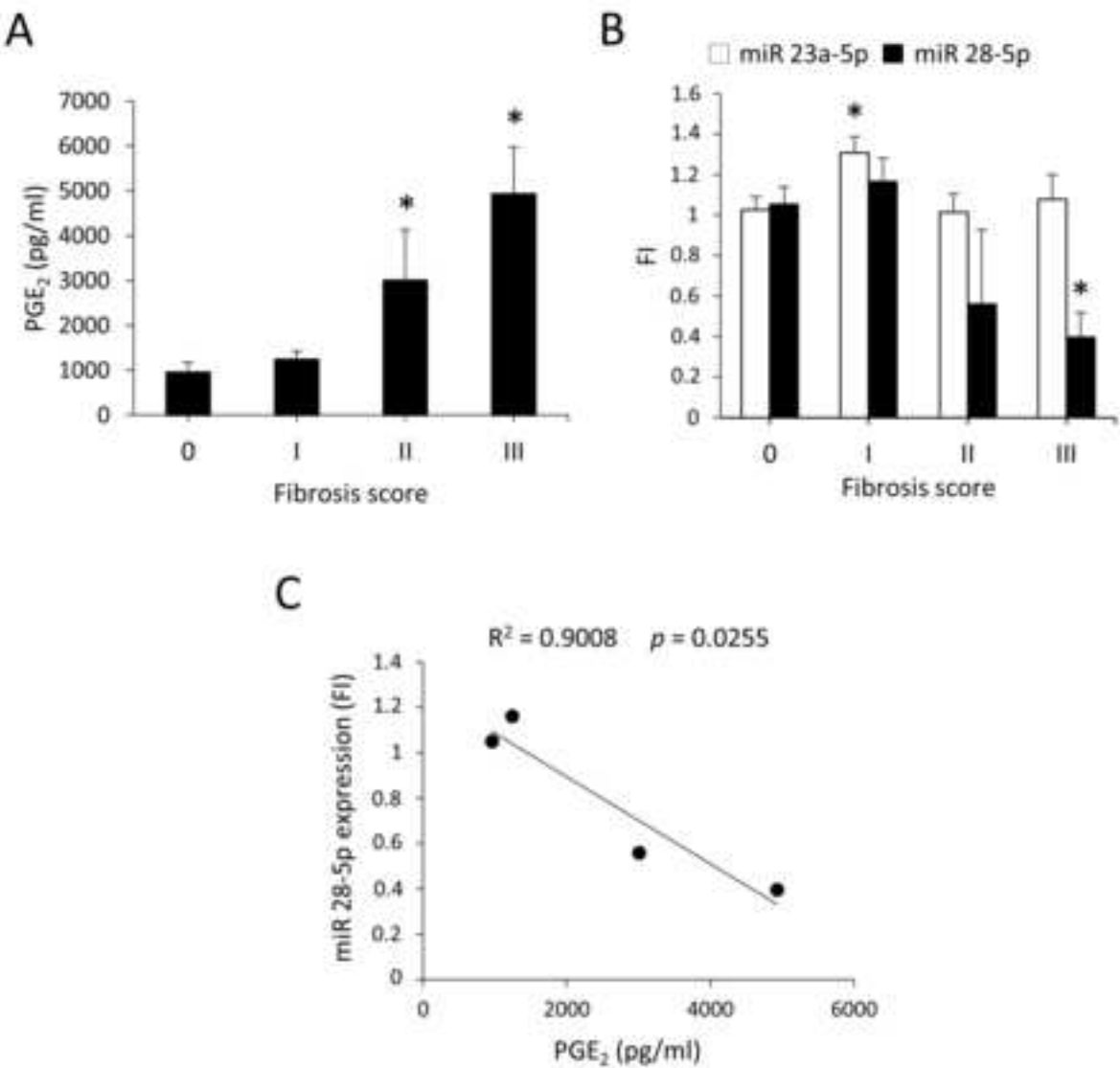
Supplementary 1
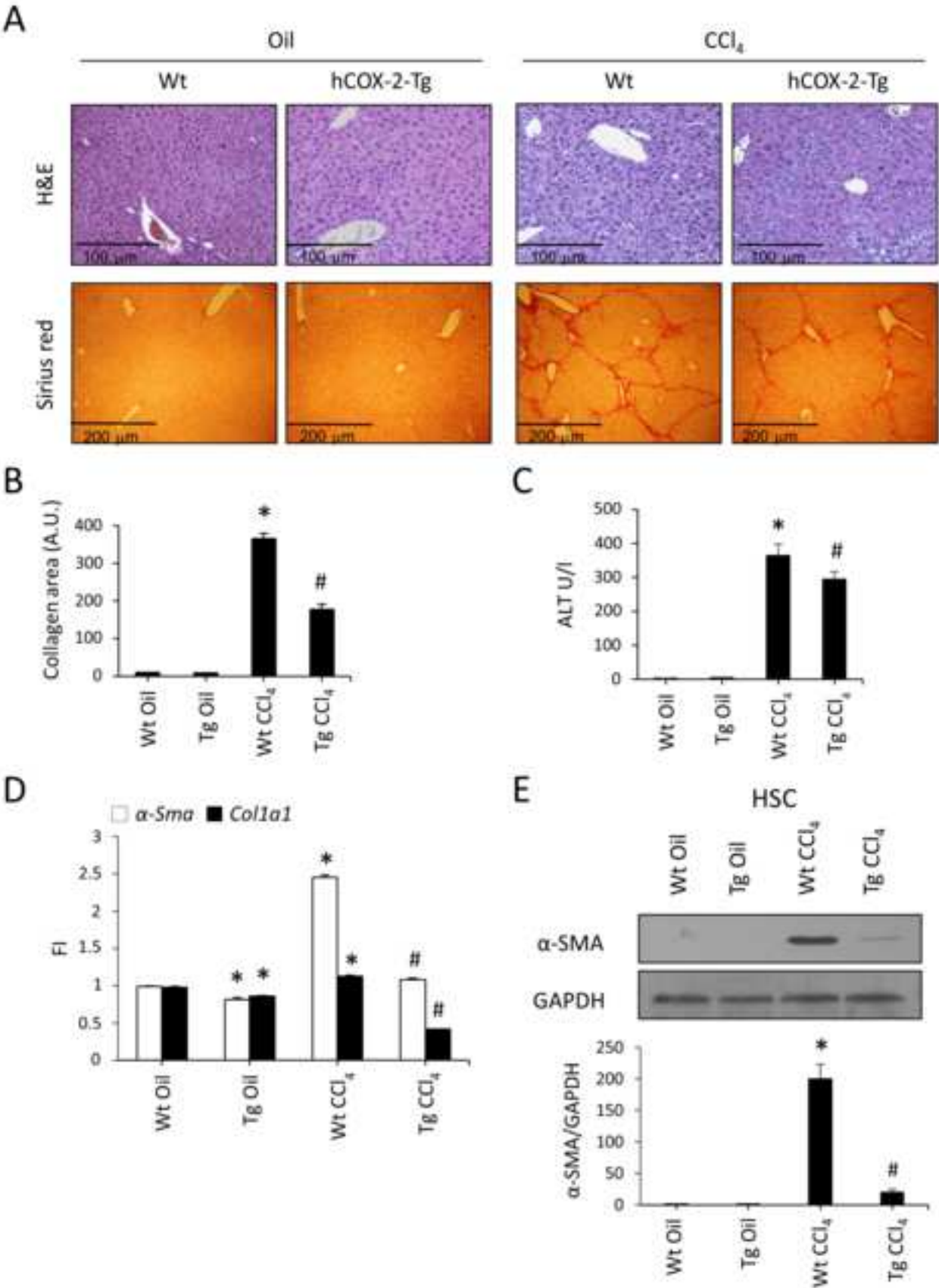
Supplementary 2
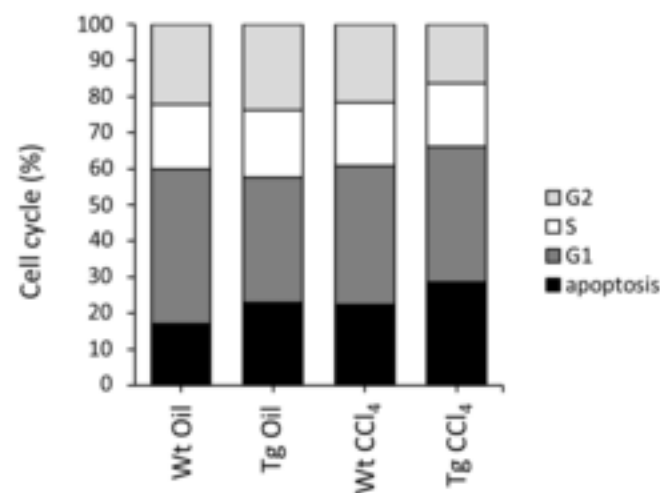
Supplementary 3

Supplementary 4

A

B

☐ miR 23a-5p   ■ miR 28-5p

C

R² = 0.9008   p = 0.0255

*Conflict of Interest Form
Click here to download Conflict of Interest Form: coi_disclosure Brea.pdf

*Conflict of Interest Form

Click here to download Conflict of Interest Form: coi_disclosure Motio.pdf

*Conflict of Interest Form

Click here to download Conflict of Interest Form: coi_disclosure Frances.pdf

*Conflict of Interest Form
Click here to download Conflict of Interest Form: coi_disclosure Garcia-Monzon.pdf

*Conflict of Interest Form
Click here to download Conflict of Interest Form: coi_disclosure Vargas.pdf

*Conflict of Interest Form
Click here to download Conflict of Interest Form: coi_disclosure Fernandez-Velasco.pdf

*Conflict of Interest Form
Click here to download Conflict of Interest Form: coi_disclosure Bosca.pdf

*Conflict of Interest Form

[Click here to download Conflict of Interest Form: coi_disclosure Casado.pdf](#)

*Conflict of Interest Form

Click here to download Conflict of Interest Form: coi_disclosure Martin-Sanz.pdf

*Conflict of Interest Form
Click here to download Conflict of Interest Form: coi_disclosure Agra.pdf

*Conflict of Interest Form
Click here to download Conflict of Interest Form: coi_disclosure Agra.pdf